

Mechanical confinement triggers glioma linear migration dependent on formin FHOD3

Pascale Monzo^{a,†,*}, Yuk Kien Chong^b, Charlotte Guetta-Terrier^a, Anitha Krishnasamy^a, Sharvari R. Sathe^a, Evelyn K. F. Yim^{a,c,d}, Wai Hoe Ng^{b,e}, Beng Ti Ang^{b,e,f,g}, Carol Tang^{b,e,h}, Benoit Ladoux^{a,i}, Nils C. Gauthier^{a,b}, and Michael P. Sheetz^{a,j,*}

^aMechanobiology Institute, National University of Singapore, Singapore 117411; ^bNational Neuroscience Institute, Singapore 308433; ^cDepartment of Biomedical Engineering, National University of Singapore, Singapore 117575; ^dDepartment of Surgery, Yong Loo Lin School of Medicine, National University of Singapore, Singapore 119228; ^eDuke–NUS Graduate Medical School, Singapore 169857; ^fYong Loo Lin School of Medicine, National University of Singapore, Singapore 117597; ^gSingapore Institute for Clinical Sciences, A*STAR, Singapore 117609; ^hHumphrey Oei Institute of Cancer Research, National Cancer Centre, Singapore 169610; ⁱInstitut Jacques Monod, Université Paris Diderot and CNRS UMR 7592, 75205 Paris, France; ^jDepartment of Biological Sciences, Columbia University, New York, NY 10027

ABSTRACT Glioblastomas are extremely aggressive brain tumors with highly invasive properties. Brain linear tracks such as blood vessel walls constitute their main invasive routes. Here we analyze rat C6 and patient-derived glioma cell motility *in vitro* using micropatterned linear tracks to mimic blood vessels. On laminin-coated tracks (3–10 μm), these cells used an efficient saltatory mode of migration similar to their *in vivo* migration. This saltatory migration was also observed on larger tracks (50–400 μm in width) at high cell densities. In these cases, the mechanical constraints imposed by neighboring cells triggered this efficient mode of migration, resulting in the formation of remarkable antiparallel streams of cells along the tracks. This motility involved microtubule-dependent polarization, contractile actin bundles and dynamic paxillin-containing adhesions in the leading process and in the tail. Glioma linear migration was dramatically reduced by inhibiting formins but, surprisingly, accelerated by inhibiting Arp2/3. Protein expression and phenotypic analysis indicated that the formin FHOD3 played a role in this motility but not mDia1 or mDia2. We propose that glioma migration under confinement on laminin relies on formins, including FHOD3, but not Arp2/3 and that the low level of adhesion allows rapid antiparallel migration.

Monitoring Editor

Yu-Li Wang
Carnegie Mellon University

Received: Aug 11, 2015

Revised: Feb 4, 2016

Accepted: Feb 18, 2016

INTRODUCTION

Studies of migration in confined spaces are relevant to embryonic development and cancer metastasis because of the natural confinement of biological environments (Friedl and Alexander, 2011). Studying migration under confinement is particularly appropriate

This article was published online ahead of print in MBoC in Press (<http://www.molbiolcell.org/cgi/doi/10.1091/mbc.E15-08-0565>) on February 24, 2016.

[†]Present address: FIRC Institute of Molecular Oncology, 20139 Milan, Italy.

*Address correspondence to: P. Monzo (pascale.monzo@ifom.eu), M. P. Sheetz (ms2001@columbia.edu).

Abbreviations used: CN, collagen; ECM, extracellular matrix; FN, fibronectin; GBM, glioblastoma multiforme; GFP, green fluorescent protein; hGPC, human glioma propagating cell; LN, laminin; RFP, red fluorescent protein; TIRFM, total internal reflection microscopy.

© 2016 Monzo et al. This article is distributed by The American Society for Cell Biology under license from the author(s). Two months after publication it is available to the public under an Attribution–Noncommercial–Share Alike 3.0 Unported Creative Commons License (<http://creativecommons.org/licenses/by-nc-sa/3.0>). “ASCB®,” “The American Society for Cell Biology®,” and “Molecular Biology of the Cell®” are registered trademarks of The American Society for Cell Biology.

for understanding glioblastoma biology. Glioblastomas (glioblastoma multiforme [GBM]) are extremely aggressive brain tumors characterized by their resistance to radiotherapy and highly invasive properties. Even with aggressive surgical resections coupled with radiotherapy and chemotherapy, the prognosis for GBM patients remains dismal (death normally occurs 3–14 mo after detection). This is because GBM cells (or grade IV gliomas) are able to rapidly migrate long distances within the brain, making complete surgical removal impossible. Blocking glioma migration would transform this brain tumor into a focal disease that would be easier to treat (Giese et al., 2003; Charles et al., 2012; Cloughesy et al., 2014; Cuddapah et al., 2014; Xie et al., 2014).

Glioma cells are generated in the brain and rarely metastasize to other tissues (Beauchesne, 2011; Hamilton et al., 2014). However, these cells are able to invade and destroy most regions of the brain, leading to the rapid death of patients. These cells do not cross the blood–brain barrier and therefore do not use the blood flow to

invade (Bernstein and Woodard, 1995). Although their intrinsic migratory properties allow glioma cells to move between neuronal axons and dendrites in the brain parenchyma, linear tracks such as white matter tracts and blood vessel walls constitute their main invasion route, suggesting that a linear geometry could play a role in their invasive properties (Nagano et al., 1993; Holash et al., 1999; Zagzag et al., 2000; Grobбен et al., 2002; Lugassy et al., 2002; Bellail et al., 2004; Farin et al., 2006; Winkler et al., 2009; Hirata et al., 2012).

In a human brain, blood vessels represent hundreds of miles of linear tracks covered with matrix proteins such as collagen, laminin, and fibronectin (Jones et al., 1982; Bellon et al., 1985; McComb and Bigner, 1985; Gladson, 1999). Moreover, they provide glucose and nutrients to surrounding cells (Zlokovic, 2008). In vitro and in vivo studies show that glioma cells actively follow blood vessels to invade the brain. In fixed tissue specimens, collections of glioma cells are frequently found around blood vessels at the infiltrative margins of tumors (Zagzag et al., 2000; Lugassy et al., 2002). Electron microscopy shows that C6 glioma cells injected in rat brains contact and spread on blood vessels (Nagano et al., 1993). Live-imaging experiments show that these cells invade almost exclusively along blood vessel paths, proliferating en route and encasing blood vessels (Farin et al., 2006; Winkler et al., 2009; Hirata et al., 2012).

On blood vessel walls, glioma cells use matrix proteins and integrin-based adhesion/migration pathways to invade (Gladson, 1999; Goldbrunner et al., 1999; Uhm et al., 1999; Lugassy et al., 2002; Farin et al., 2006; Winkler et al., 2009; Lathia et al., 2010; Hirata et al., 2012). Laminin seems to play a specific role in glioma migration. It is enriched in and around the tumor, particularly around blood vessels (McComb and Bigner, 1985). Moreover, integrin expression studies have underlined potential roles for the laminin receptors $\alpha 2\beta 1$, $\alpha 3\beta 1$, $\alpha 6\beta 1$, and $\alpha 6\beta 4$ in glioma invasion (Paulus et al., 1993; Gingras et al., 1995; Chintala et al., 1996; Previtali et al., 1996; Tysnes et al., 1996; Haugland et al., 1997; Knott et al., 1998; Belot et al., 2001; Bellail et al., 2004; Hwang et al., 2008; Delamarre et al., 2009; Lathia et al., 2010).

On blood vessel walls, glioma cells adopt a specific mode of migration that is different from their motility in the parenchyma (Hirata et al., 2012). On blood vessel walls, glioma cells migrate faster and in a saltatory manner and display a unipolar elongated morphology, as opposed to their multipolar morphology observed in the parenchyma (Farin et al., 2006; Beadle et al., 2008; Ivkovic et al., 2012). Moreover, on blood vessels, glioma cells display lower Rac1 and CDC42 activities and higher RhoA activity than in cells migrating in the parenchyma (Farin et al., 2006; Winkler et al., 2009; Hirata et al., 2012). These observations indicate that glioma cells can switch from a slow, random migration mode (Rac and CDC42 dependent) when navigating in the parenchyma to a fast migration mode (Rho dependent) when streaming on linear blood vessels.

In the present study, we analyze the migration of rat C6 glioma cells and of human glioma-propagating cells (hGPCs) isolated from a patient, two cell lines that migrate efficiently in murine brains (Farin et al., 2006; Hirata et al., 2012; Ng et al., 2012). We use micropatterning techniques to mimic blood vessel wall confinement. Using total internal reflection fluorescence microscopy and long-term imaging, as well as expression and phenotypic analysis, we find that formin proteins play an important and specific role in glioma linear migration.

RESULTS

C6 glioma cells migrate efficiently on linear laminin tracks

Fibronectin, collagen, and laminin are the most common extracellular matrix (ECM) proteins that have been localized to blood vessels

or perivascular tissue in glioma (Jones et al., 1982; Bellon et al., 1985; McComb and Bigner, 1985; Gladson, 1999). They all have been used in studies of glioma motility with various glioma cell lines (e.g., Grau et al., 2015; Rape et al., 2015; Wong et al., 2015). To clarify which substrate was the most efficient to stimulate motility in C6 glioma cells, we compared these three substrates side by side. On glass-bottom dishes coated with these matrix proteins at three different substrate concentrations (10, 50, and 100 $\mu\text{g/ml}$), we found that laminin supported better migration of C6 glioma cells than either collagen or fibronectin, indicating that laminin substrates were preferred for migration (Figure 1, A, B, and D, and Supplemental Movie S1). On two-dimensional (2D) laminin-coated surfaces, C6 cells moved randomly, with the formation of a broad lamellipodium, and changed direction frequently. Long tails formed at the rear of cells and extended occasionally over 50–120 μm in length (Figure 1B; white arrows; Supplemental Figure S3Ba). To better approximate the laminin topology in the brain, we stamped thin lines (width varying from 3 to 7 μm) of laminin onto Petri dishes. As shown in Figure 1, C and E, C6 cells moved more rapidly along the lines (more than two times faster than in two dimensions), adopting a spindle shape with long leading processes (see also Supplemental Movies S2 and S3 and Supplemental Figure S1). This elongated spindle shape was similar to the “elongated unipolar shape” observed in vivo when C6 cells migrated along blood vessel tracks (Farin et al., 2006; Beadle et al., 2008).

Glioblastoma linear migration is saltatory and involves paxillin-containing adhesions

C6 glioma cells exhibited saltatory migration on microfabricated laminin tracks similar to their motion in the brain (Farin et al., 2006; Hirata et al., 2012; Figure 2, A and B, and Supplemental Movie S2). Detailed analyses revealed that movement involved two phases: 1) cell elongation and 2) tail retraction. In phase 1, cells extended leading processes with small lamellipodia at a constant speed ($63 \pm 8 \mu\text{m/h}$; $n = 10$), but the cell body moved forward at a slower speed ($52 \pm 4 \mu\text{m/h}$; $n = 10$), causing elongation of the cell. Further, the tail often extended rearward, and that further elongated the cells (Figure 2, A and B, and Supplemental Movie S2). Glioma cells migrating on thin laminin lines were able to change direction from time to time ($18 \pm 4.3\%$ of cases). When changes in direction occurred, the tail became the leading edge (Figure 2C and Supplemental Movie S3). To analyze adhesion and actin dynamics in the first phase (elongation), we transfected C6 cells with green fluorescent protein (GFP)-actin and red fluorescent protein (RFP)-paxillin or Arp3-mCherry and monitored the distribution of fluorescence at the cell/matrix interface with total internal reflection fluorescence microscopy (TIRFM). Paxillin-containing adhesions were observed as small patches 2 μm in length at both the leading edge and the tail. In addition to the cell leading edge, small lamellipodia containing Arp2/3 also formed on the sides of the cell as well as the rear, indicating that the cell was scanning its environment along its entire length (Figure 2, D and E, and Supplemental Movies S4 and S5).

During the second phase, the cell restored its original length by sudden retraction of the tail, rapid movement of the cell body forward ($147 \pm 16 \mu\text{m/h}$; $n = 10$), and constant leading-edge movement ($63 \pm 8 \mu\text{m/h}$; $n = 10$). During tail retraction, paxillin-containing adhesions disassembled. Of interest, before adhesion disassembly, some paxillin-containing adhesions elongated while nearby, smaller adhesions disappeared (Figure 2E, zoom, and Supplemental Movie S5). It appeared that increased contractile forces caused the slip, clustering, and eventual disassembly of adhesions. Tracking analysis during tail retraction revealed that 50% of the adhesions were sliding in the

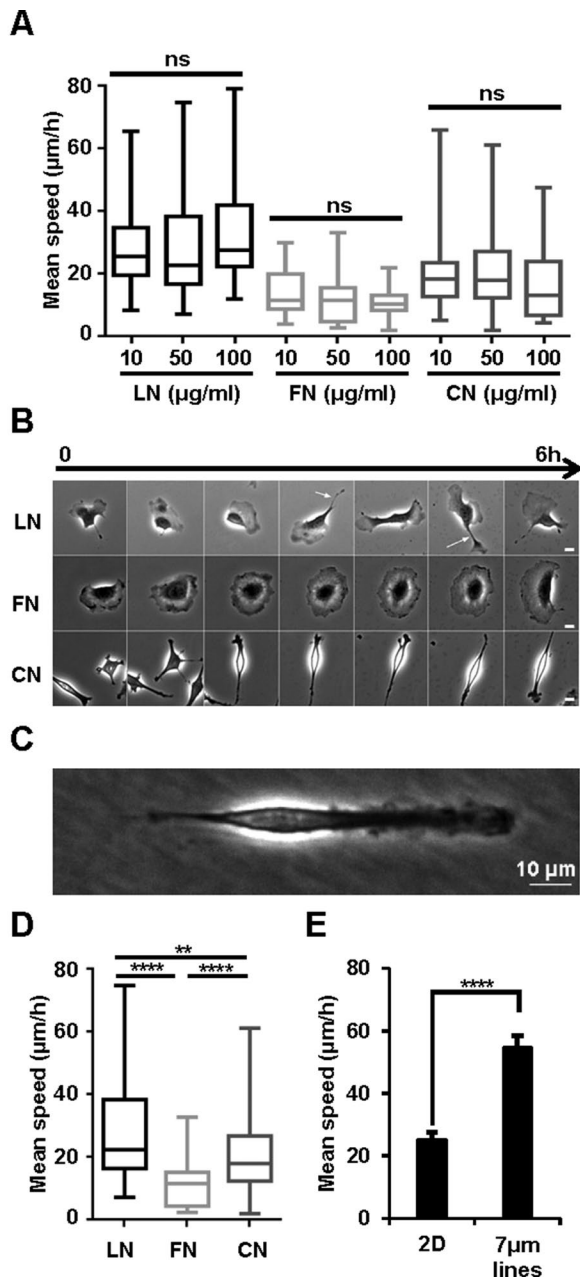


FIGURE 1: Comparison of C6 glioma cell motility on different substrates. C6 glioma cells were plated on glass-bottom dishes coated with 10, 50, or 100 µg/ml laminin (LN), fibronectin (FN), or collagen (CN). Cells were imaged in phase contrast (1 image/6 min). Error bars are SDs. (A) Average of mean speed (µm/h) on each substrate. (B) Glioma cells adopt different shapes when seeded on different substrates (50 µg/ml). Montage showing snapshots of single cells during 6 h (1 frame/h). Scale bars, 10 µm. (C) Typical snapshot of a C6 glioma cell migrating on thin laminin micropatterned line. (D) Average of mean speed (µm/h) on laminin, fibronectin, and collagen at 50 µg/ml. Error bars are SD. (E) Average of mean speed (µm/h) on laminin-coated dish (2D) and 7-µm laminin micropatterned lines (7-µm lines). Error bars are SEM. *p* values were calculated using unpaired *t* tests.

direction of the cell movement and gathered together in bigger clusters before being ripped off. At the front of the cell, adhesion tracking revealed that most of the adhesions were stationary and traversed most of the cell length before disassembling (see adhesion track projections in Supplemental Figure S2 and Supplemental Movie S6).

Thus geometric confinement caused a switch from 2D random migration to an efficient two-phase, linear migration mode that was saltatory, similar to neuronal and glioma motility described *in vivo*, presenting small lamellipodial protrusions with paxillin-containing adhesion patches (Beadle *et al.*, 2008; Ivkovic *et al.*, 2012). This behavior was also reminiscent of the motility of fibroblasts on thin lines of fibronectin or gelatin (Doyle *et al.*, 2009, 2012; Guo and Wang, 2012; Chang *et al.*, 2013).

Mechanical constraint caused by increased cell density triggers glioma linear migration

Blood vessel diameter can vary greatly, ranging from 5 to 10 µm for the capillaries to 25 mm for the biggest arteries. In the brain, blood vessels can accommodate several rows of glioma cells that keep growing and overcrowd the surface. To understand how these cells can migrate in such a highly packed linear environment, we used a range of lines of bigger sizes and looked at the migration of dense glioma cell populations. The pattern we used had a large continuous region of laminin (reservoir) connected to 12 lines of different widths varying from 10 µm (line 1) to 400 µm (line 12; Figure 3A, Supplemental Figure S3A, and Supplemental Movies S7 and S8; Vedula *et al.*, 2012, 2014). Cells migrated spontaneously in the reservoirs, as well as on the lines, with a mean speed average of ~30 µm/h (Supplemental Figure S1). In the reservoirs, they adopted a 2D random motion similar to their motion on glass-bottom dishes described in Figure 1B (Supplemental Figure S3Ba). On the narrow lines, cells migrated in anti-parallel arrays, resembling bidirectional currents (Figure 3B, Supplemental Figure S3B, b and c, and Supplemental Movies S7 and S8). Tracking analysis showed a high persistency of migration (>0.8) in most of the lines (Figure 3, B and D, and Supplemental Movie S9). On larger lines, cells initially migrated in all directions similar to the reservoir, but over time, the lines became more crowded and cells oriented parallel to the line axis and moved in a linear migration mode with high persistency (see montages in Figure 3E and Supplemental Movie S8). This indicated that increasing cell density could trigger coordinated antiparallel linear migration. We measured cell density, persistency, and speed on line 10 (130 µm) as a function of the time. At the beginning of the movie (0–6 h), cell density progressively increased from 1000 to 1500 cells/mm², in the middle part of the movie (6–12 h) from 1500 to 1660 cells/mm², and toward the end of the movie (12–18 h) from 1660 to 1960 cells/mm² (Figure 3F). At the beginning of the movie, the population was evenly distributed between cells with high and low persistency as well as high and low migration speed (Figure 3G and Supplemental Figure S3C). Most of the cells became persistent only in the second part of the movie (6–12 h) when cell density reached the threshold of 1500 cells/mm², with the fastest cells being the most persistent (Figure 3H and Supplemental Figure S3C). The persistency continued even at higher cell density (12–18 h; Figure 3E and Supplemental Figure S3C). The fast and persistent cells were often observed on the edge of the line (see also tracks of lines 11 and 12 in Figure 3B) and migrated at a similar speed to that of single cells on thin lines (~50 µm/h). They also displayed a similar elongated spindle shape (Supplemental Figure S3B, b and c).

To track the movement of single cells within a crowded line, we transfected glioma cells with a plasma membrane marker coupled to GFP (GFP-PM) or GFP only and followed the fluorescent cells moving among untransfected cells on the lines (Figure 3, J and K, and Supplemental Movies S10 and S11). Similar to the isolated cells migrating on thin lines, cells migrating on large lines used a saltatory linear

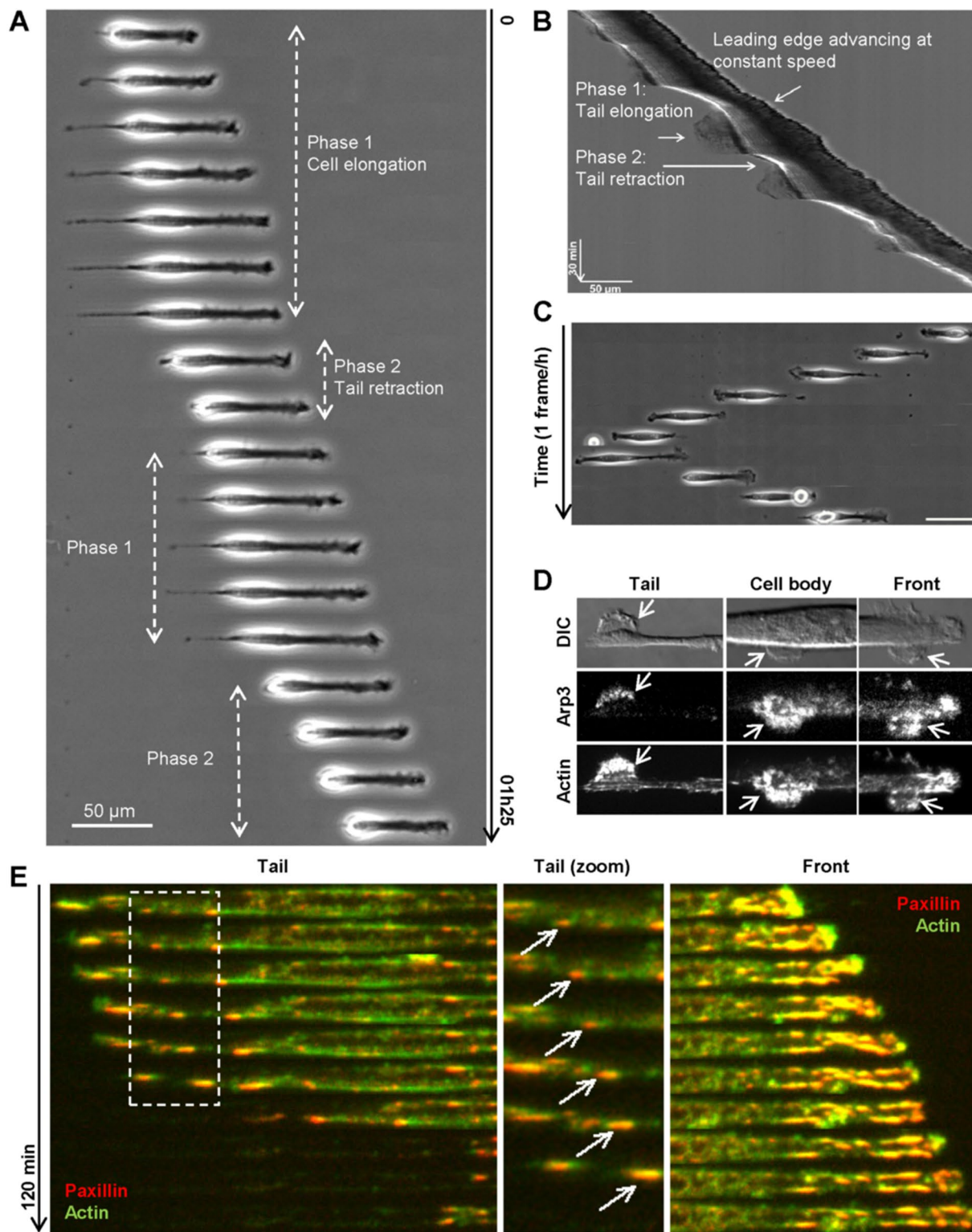


FIGURE 2: Confined linear migration is saltatory and involves a leading process and a searching tail both containing adhesive patches and small lamellipodia. (A, B) Glioma cells were seeded on laminin-coated lines of 3- μm width and imaged every 30 s. (A) Montage corresponding to 90-min total time. (B) Kymograph corresponds to total time 3 h, 30 min; frames are 30 s apart. (C) Glioma cells were seeded on laminin-coated lines of 3- μm width and imaged every 6 min. Montage corresponds to 9-h total time. (D) Glioma cells transfected with GFP-actin and Arp3-mCherry were seeded on laminin-coated lines of 5- μm width and imaged using a TIRF microscope. Images extracted from the Supplemental Movie S4 showing the presence of Arp2/3 in lamellipodia protruding at the front, tail, and cell body. (E) Glioma cells transfected with GFP-actin and mCherry-paxillin were seeded on laminin-coated lines of 3- μm width and imaged using a TIRF microscope. Montage corresponds to 120-min total time. Paxillin-containing adhesions are present in the leading process and in the tail as noticeable patches 2 μm in length.

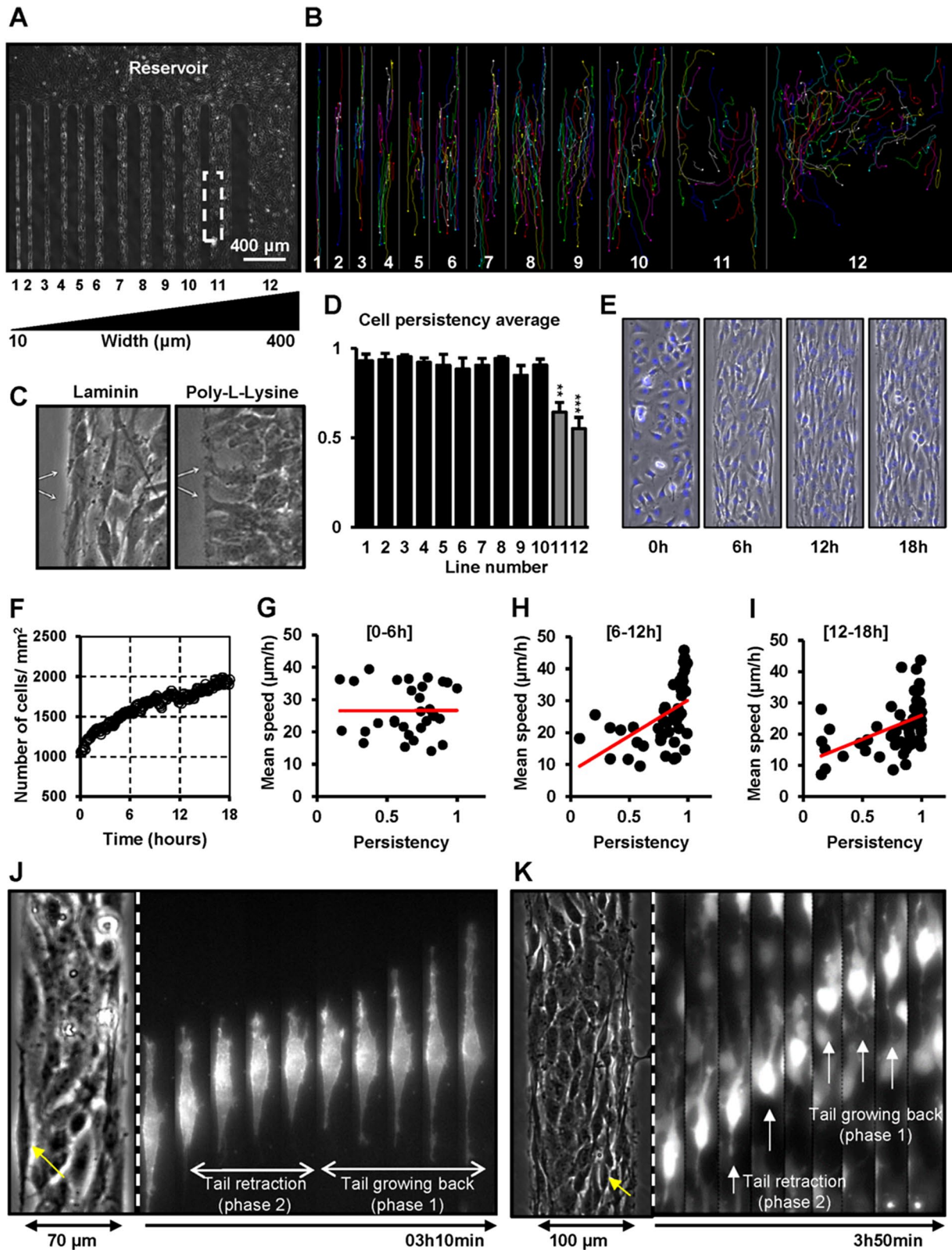


FIGURE 3: Mechanical constraint mediated by an increase in cell density triggers glioma linear migration. C6 glioma cells were plated on lines of laminin of different widths, varying from 10 μm (line1) to 400 μm (line12), and connected to a large reservoir. Cells were imaged after 1-h seeding for long periods of time in phase contrast using a 10 \times objective (1 image/6 min). (A) Reconstitution of the entire pattern at the end of the movie (24 h). (B) Tracks of the cell bodies during 6 h. (C) Comparison of C6 glioma cell behavior at the edge of lines coated with laminin (left) or poly-L-lysine (right). (D) Persistency average of C6 glioma cells migrating on each laminin-coated line. (E) Montage showing the transition from a 2D migration to the linear migration as the cell density increases on line 10 (130- μm width) over time. Frames are 6 h apart. Montage extracted from Supplemental Movie S8. (F) Cell density was measured on line 10 and is

migration mode (Figure 3, J and K, and Supplemental Movies S10 and S11). This was observed for cells on the edge as well as in the middle of lines (Figure 3, J and K).

These results showed that the linear migration mode can occur on both thin and overcrowded, thick lines. On thick lines, the linear motion propagated from the side of the lines toward the center when cell populations reached a density threshold of 1500 cell/mm².

To determine whether this behavior depended on laminin, on the confinement, or on the proximity of nonadhesive edges, we monitored glioma cell behavior on poly-L-lysine-coated lines. In contrast to the laminin substrates, cells seeded on poly-L-lysine-coated lines aligned perpendicularly to the edge of all lines and reservoirs and did not migrate at all (Figure 3C, Supplemental Figure S4, and Supplemental Movie S12). This result demonstrated that the confinement and geometry were not sufficient to trigger the streaming coordinated linear motion but that the laminin substrate was required. Taken together, these results showed that geometric and density confinement on laminin activated a linear migration mode.

To further demonstrate that confinement (i.e., reducing the available space to force the cells to adapt their shape) was necessary and that linear geometry coupled to laminin was not sufficient, we seeded glioma cells on laminin-coated fabricated lines 2 μm in width and separated by 2 μm from the next 2-μm line by a recessed region (Figure 4, A–C). Similar to previous studies (Clark *et al.*, 1990; Curtis and Wilkinson, 1997; Dalton *et al.*, 2001; Teixeira *et al.*, 2003; Hamilton *et al.*, 2010), cells did not penetrate grooves of this depth and relied on the upper surface. On these patterns, cells migrated on the lines and were not confined but were able to sense the geometry. Indeed, cells migrated in a directed manner parallel to the direction of the lines (Figure 4D and Supplemental Movie S13). However, they adopted a 2D migration mode, as shown by the flat shape of the nuclei, their broad lamellipodia (Figure 4E), and slower velocity than during the linear migration mode on thin lines (Figure 4F and Supplemental Movie S13).

Thus three parameters of the blood vessel surface were sufficient to reproduce *in vivo* the saltatory mode of motility (Farin *et al.*, 2006; Hirata *et al.*, 2012): 1) linear geometry, 2) high cell density (i.e., confinement), and 3) laminin coating.

Linear migration involves contractile, longitudinal actin cables regulated by formin and myosin II activity but not Arp2/3

To understand the importance of the actin and microtubule cytoskeleton in the 2D and linear modes of migration, we used specific inhibitors with acute effects (Figure 5 and Supplemental Movies S14 and S15). Drugs were added after cell migration started (~3 h after seeding). Cells were imaged by phase contrast under the same conditions as in Figures 1 and 3 and tracked for at least 6 h. Both types of glioma cell movement slowed down significantly upon latrunculin A addition. Blebbistatin also caused a large decrease in velocity in both migration modes (Figure 5C). Blebbistatin or latrunculin A addition caused similar alterations in cell shape, with cells extending extremely thin processes (Figure 5, A and B). Nocodazole addition severely inhibited motility by blocking polarization of the cells;

reported as a function of time. (G, H) Cell persistency and mean speed measured on line 10 in three different time windows. Best-fit lines are in red. $R = 0.003$ (G), 0.509 (H), and 0.446 (I). (J) GFP-PM-transfected cells were mixed with untransfected cells and seeded on laminin-coated lines of different sizes. GFP signal was used to follow the edges of the cells when streaming. Montage corresponds to 3 h, 10 min total time. Frames are 20 min apart. (K) C6 cells expressing GFP were seeded on 100-μm-wide laminin-coated lines and imaged in fluorescence and phase contrast using a 20× objective (1 image/10 min). Montage showing a cell using saltatory motility while migrating in the middle of the line. Frames are 30 min apart.

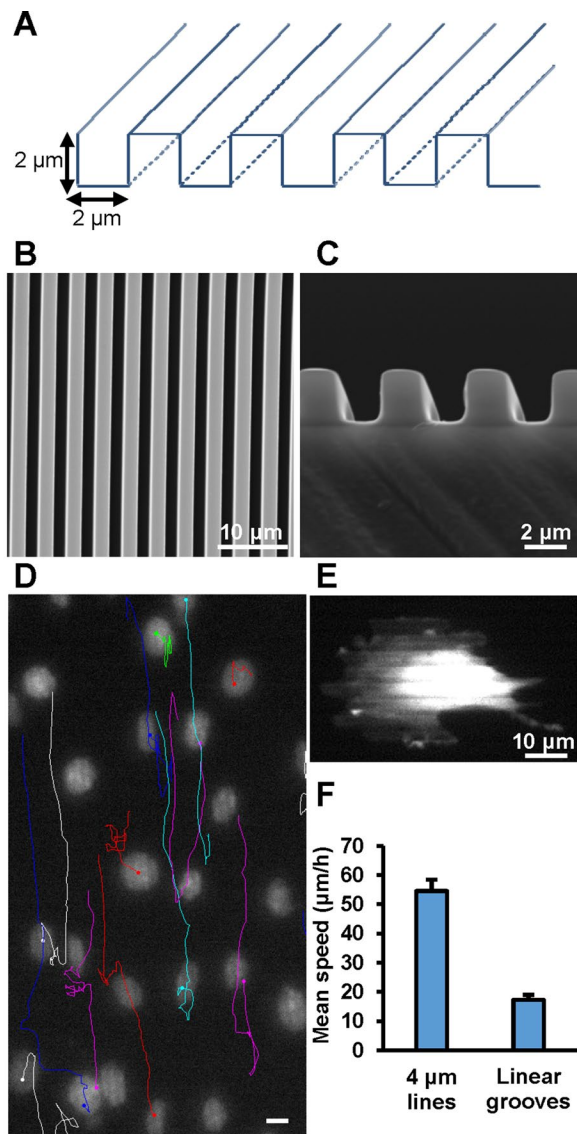


FIGURE 4: Confinement is necessary to trigger glioma linear migration. (A) Schematic of the fabricated linear grooves. Scanning electron micrograph (B) and cross-sectional scanning electron micrograph (C) of fabricated linear grooves (2 μm × 2 μm × 2 μm). (D) C6 glioma cells preincubated with Hoechst 33342 were plated on the laminin-coated fabricated linear grooves and imaged for 15 h (1 image/6 min). Image shows the overlay of the tracks and nuclei at the end of the movie. (E) Micrograph of a GFP-transfected cell migrating on top of the linear grooves. (F) Mean speed comparison of cells migrating on 4-μm lines and the fabricated linear grooves.

cell size shortened, but lamellipodial activity persisted (Figure 5 and Supplemental Movie S14). Of interest, small doses of nocodazole (0.1 μM) were sufficient to block the migration, similar to previous observations in two dimensions (Panopoulos *et al.*, 2011).

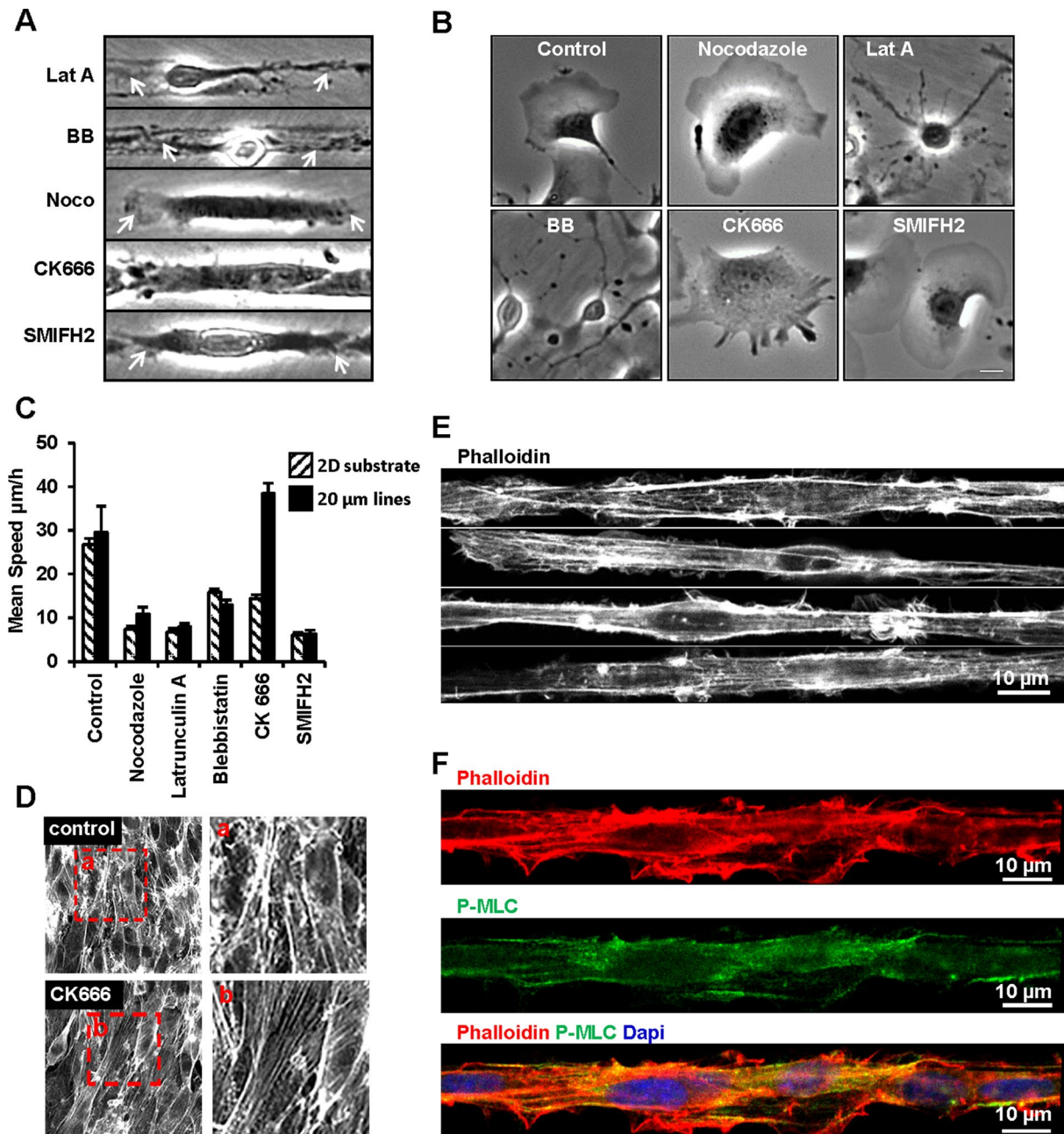


FIGURE 5: Linear migration mode involves contractile longitudinal actin cables dependent on formin but not Arp2/3. (A–C) C6 glioma cells were plated on a 2D flat surface and laminin lines of different widths. Cells were imaged for long periods of time (15–20 h) in the presence of different drugs: blebbistatin (50 μM), latrunculin (1.2 μM), nocodazole (0.1 μM), CK666 (100 μM), and SMIFH2 (20 μM). (A) Snapshots showing the effects of the drugs on the shape of the cells migrating on 10- μm lines. (B) Snapshots showing the effects of the drugs on the shape of the cells migrating on 2D surface (sparse condition). (C) Average of mean velocities ($\mu\text{m/h}$) over 6 h. Error bars represent SEM. (D) C6 glioma cells in the reservoir control or after CK666 treatment. Actin filaments were stained with Alexa 568–phalloidin and imaged using a confocal microscope. Treated cells on bottom show noticeable parallel actin bundles compared with control cells on the top. (E, F) Confocal images of glioma cells migrating on 20- μm lines fixed and stained for phospho–myosin light chain 2 (Ser-19) and phalloidin. Bars, 10 μm .

Microtubules appeared to be important for the polarization of the motility and growth of leading processes but not for lamellipodial activity. Confocal images of C6 glioma cells stained with phalloidin on crowded 10- μm -wide lines revealed longitudinal actin bundles extending the full length of the cells (Figure 5E). These actin bundles were decorated with active phospho–myosin II all along their length (Figure 5F). Active phosphomyosin was also enriched around the

nuclei and at the back of the leading process (Supplemental Figure S5A), which indicated primary sites of contractility. Active phospho–myosin II was also found along stress fibers and at the cytokinetic ring of dividing cells (Supplemental Figure S5B), indicating that the antibody was giving a specific signal (Beadle *et al.*, 2008; Keil *et al.*, 2009). There are two major mechanisms of actin polymerization: Arp2/3–N-WASP– or formin–dependent polymerization. Surprisingly,

linear migration was not dependent on Arp2/3. Instead, the Arp2/3 inhibitor CK666 caused an increase in the linear migration velocity on thick lines, whereas it inhibited 2D random motion (Figure 5C and Supplemental Movies S14 and S15). On 2D surfaces at low cell densities, CK666 treatment caused an indentation of lamellipodia and a decrease in velocity (Figure 5, B and C). In contrast, at high densities on the large lines that activated the linear migration mode, CK666 addition caused sharper spindle shapes, better alignment in antiparallel arrays even in the reservoir (Figure 5D), and higher velocities of migration. In contrast, addition of the formin inhibitor SMIFH2 (Rizvi *et al.*, 2009) completely blocked 2D and linear migration by inhibiting process extension (Figure 5, A and C). After SMIFH2 addition, on 2D surfaces at low cell densities, glioma cells developed large lamellipodia all around their periphery and were not able to polarize in any direction (Figure 5, B and C, and Supplemental Movie S14). On the linear patterns, SMIFH2 addition blocked all process extension and migration (Figure 5, A and C, and Supplemental Movie S15). This indicated that formins catalyzed actin filament assembly for process extension in the linear migration mode and could organize actin bundles all along the leading process.

Linear migration mode in human glioma-propagating cells

We examined whether this linear type of motility was used by human glioma cells. For this purpose, we used a glioma-propagating cell line isolated from a glioblastoma patient showing highly invasive glioblastoma (Chong *et al.*, 2009, 2015; Ng *et al.*, 2012). These cells were grown as tumor spheres without serum and were able to invade murine brains with great efficiency, reflecting the clinical observations. As observed in Figure 6, A and B, and Supplemental Movie S16, these human GPCs were able to adhere and migrate on laminin substrates similar to C6 cells, whereas fibronectin did not stimulate migration. Unlike C6 cells, human GPCs were not able to adhere to collagen and stayed in suspension as tumor spheres. These cells adopted a spindle shape (Figure 6D) and migrated readily on laminin-coated lines in a saltatory manner (Figure 6E and Supplemental Movie S17). Similar to the rat C6 glioma cells, human GPCs migrating on laminin-coated lines were not affected by Arp2/3 inhibition, whereas formin inhibition using SMIFH2 completely blocked their migration (Figure 6C).

Localization, expression, and knockdown of formins in rat C6 glioma cells and human GPCs support a role for the formin FHOD3 in migration on linear laminin patterns

Because the formin inhibitor blocked linear migration in both glioma cell lines, we tested antibodies to a number of formins in order to identify the formins involved in glioma linear migration. We compared the expression levels of six different formins by Western blotting in glioma cells and two other rat cell lines—undifferentiated PC12 and rat embryonic fibroblasts REF52 (Figure 7A). Each cell line expressed a different set of formins. PC12s expressed more FMNL1, whereas REF52 expressed more mDia1 and FHOD1. C6 glioma cells expressed all of the formins tested: mDia1, mDia2, FMNL1, FMNL2, FHOD1, and FHOD3. In particular, the levels of mDia2 and FHOD3 were higher than in the other cell lines, indicating that these two formins could be specifically involved in glioma migration. Moreover, FHOD3 and mDia2 were also present in human GPCs, again supporting a role for these two formins in glioma motility (Supplemental Figure S6, A–C). We then examined their involvement in glioma linear migration using knockdown experiments (Figure 7, B–E, Supplemental Figure S6, and Supplemental Movie S19). Because mDia1 was also expressed by the two cell lines and has been involved in C6 glioma 2D migration (wound healing) and

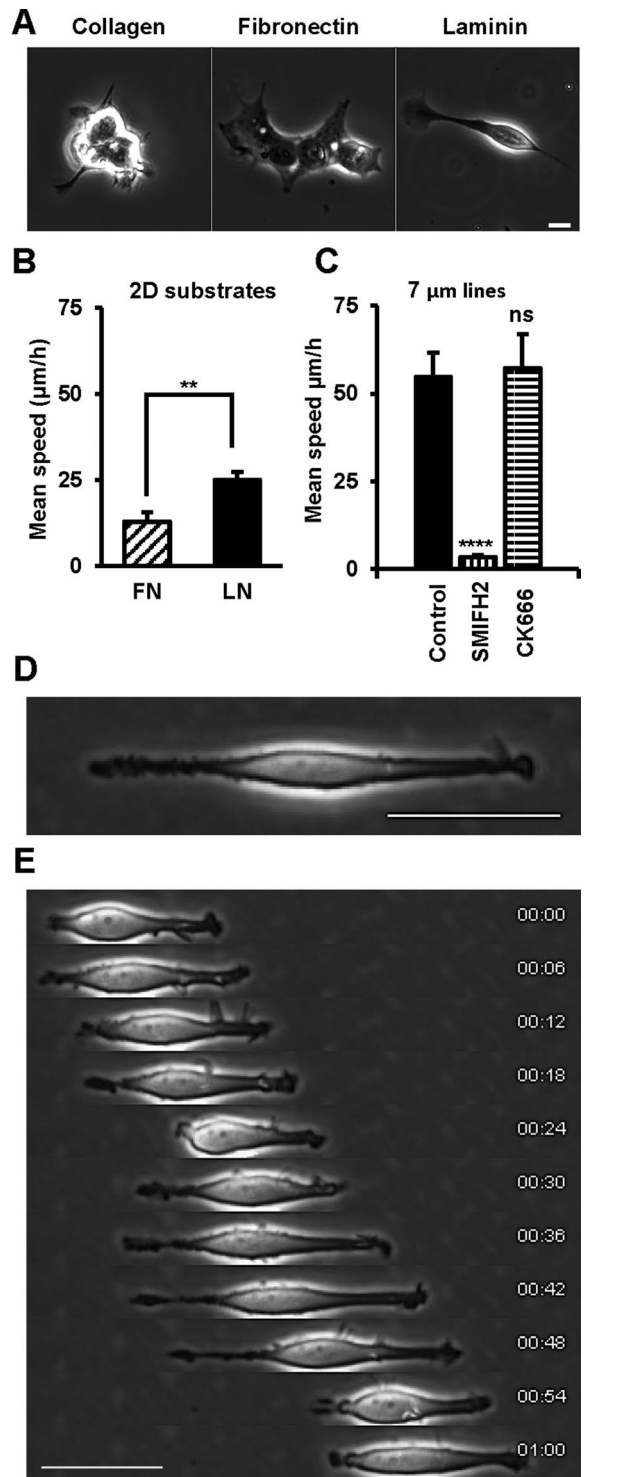


FIGURE 6: Linear migration mode in hGPCs. hGPCs were seeded on glass-bottom dishes coated with 50 μg/ml laminin, fibronectin, or collagen. Cells were imaged in phase contrast for 6 h (1 image/6 min). (A) Snapshots of hGPCs adopting different shapes when seeded on different substrates. Scale bar, 10 μm. (B) Average of mean speed (μm/h) over 6 h on fibronectin (FN) or laminin (LN). (C) HGPCs were seeded on 7-μm laminin-micropatterned lines. Cells were imaged in the presence of CK666 (200 μM) or SMIFH2 (10 μM). Average of mean speed (μm/h) over 6 h. Error bars are SEM. (D) Typical snapshot of hGPCs migrating on a 7-μm laminin micropatterned line. Scale bar, 50 μm. (E) Montage corresponds to 60-min total time; frames are 6 min apart. Scale bar, 50 μm.

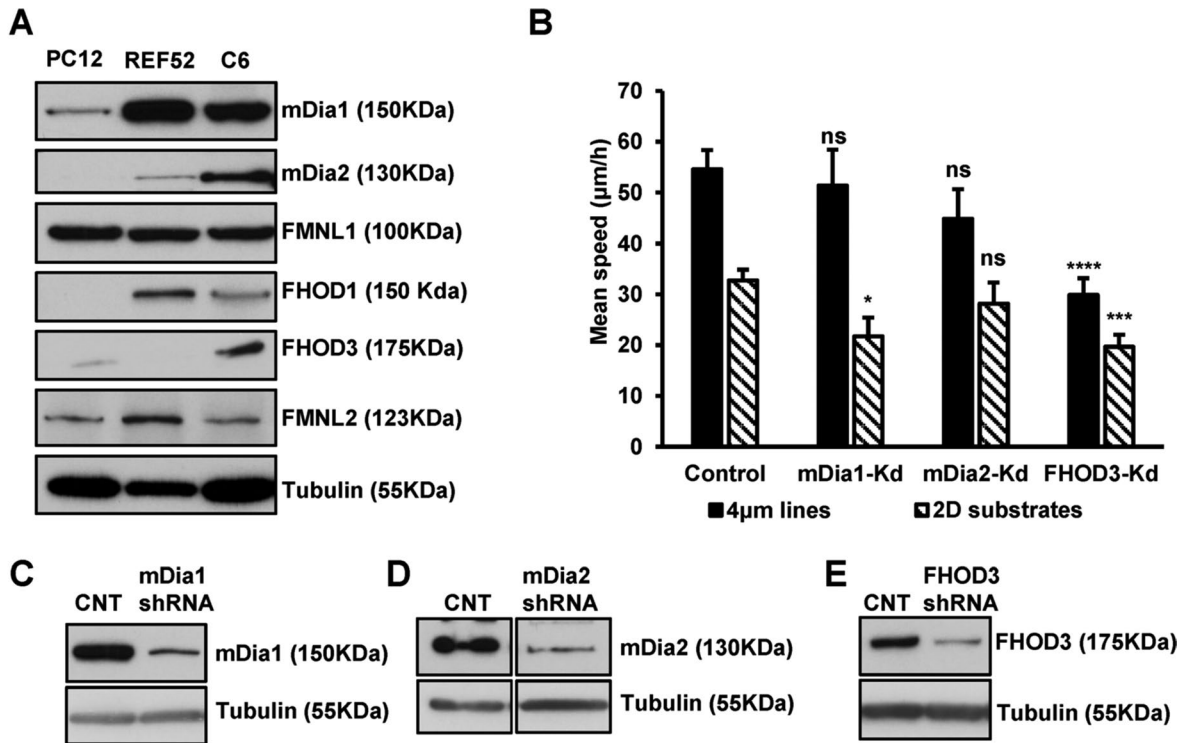


FIGURE 7: Expression profile and knockdown of formins in rat C6 glioma cells suggest a role for FHOD3. (A) Expression of formins in cell extracts (30 µg) from three different rat cell lines—PC12, REF52, and C6 glioma—was examined by Western blotting with antibodies against mDia1, mDia2, FMNL1, FHOD1, FHOD3, and FMNL2. α -Tubulin was used as a loading control. (B) C6 glioma cells were transfected with shRNA targeting mDia1, mDia2, and FHOD3. Three days later, transfected cells were seeded on 4-µm laminin micropatterned lines and 2D substrates and imaged for 6–12 h. Average of mean speeds (µm/h) over 6 h. Error bars are SEM. (C–E) Expression of mDia1, mDia2, and FHOD3 in shRNA-transfected cells was examined by Western blotting with antibodies against mDia1, mDia2, and FHOD3. α -Tubulin was used as a loading control.

three-dimensional (3D) migration (Transwell; Yamana *et al.*, 2006), we also tested whether mDia1 was involved in glioma linear migration. We transfected human GPCs and rat C6 cells with short hairpin RNA (shRNA) targeting human or rat mDia1, mDia2, and FHOD3 cloned in GFP-expressing vectors. Three to four days after transfection, GFP-expressing cells were assayed for their ability to move along thin laminin lines (4–7 µm) and in two dimensions in comparison to shRNA control-transfected cells (Supplemental Movies S18 and S19). Protein knockdown levels were estimated by Western blot (see Figure 7, C–E, for rat C6 and Supplemental Figure S6, A–C, for hGPCs) and varied between 40 and 90% knockdown, depending on the formin and the transfection efficiency (see Supplemental Figure 6, D and F, for knockdown quantification). In both cell lines, knockdown of FHOD3 reduced the migration speed on linear patterns (Figure 7B and Supplemental Figure S6E) by a factor of two, whereas the effects of knocking down mDia1 or mDia2 were not significant compared with control conditions. However, the speed on 2D substrates was affected by FHOD3 and mDia1 knockdown, as observed by Yamana *et al.* (2006). In addition, we observed that FHOD3-knockdown cells moved slowly and stayed close to each other instead of spreading and exploring their environment as did control and most of the mDia1- and mDia2-knockdown cells. In several cases, we observed clusters of cells that would not dissociate on laminin. In other cases, single migrating cells attached to nearby cells, and the migration was slowed (Supplemental Movie S18). In the case of mDia1 knockdown, a minor population of mDia1-knockdown cells moved extremely slowly (mean speed, <10 µm/h),

whereas the majority of the knockdown population moved at approximately the same speed as the control (mean speed, >20 µm/h; Supplemental Figure S6G). This reflected either heterogeneity in the knockdown population or a compensatory effect in the majority of the cells. The consistently lower migration velocity in the FHOD3-knockdown cells indicated that it had a major role in the migration process. GFP-FHOD3 was detected on parallel actin filaments found in leading processes during linear migration but not at the tips of lamellipodia (Figure 8A), suggesting that FHOD3 was involved in the generation and/or bundling of parallel actin cables that support spindle-shaped cells. In accordance, GFP-FHOD3-overexpressing cells displayed excessive amounts of longitudinal actin bundles (Figure 8B; see also Supplemental Figure S7).

DISCUSSION

We find that the confinement of glioma cells (by either crowding or substrate patterning) leads to a very efficient process of migration on laminin tracks that is similar to *in vivo* observations in rat brains (see model in Figure 9; Farin *et al.*, 2006; Beadle *et al.*, 2008; Winkler *et al.*, 2009; Hirata *et al.*, 2012). When glioma cells become confined to the laminin tracks, they switch from 2D random motion to efficient linear migration. During this linear migration, antiparallel flows of cells are observed along the axis of the laminin tracks. Within these flows, each individual cell moves by a two-phase saltatory process that depends on microtubules and contractile actin bundles in a process similar to *in vivo* saltatory migration of glioma cells (Farin *et al.*, 2006; Beadle *et al.*, 2008; Ivkovic *et al.*, 2012). The

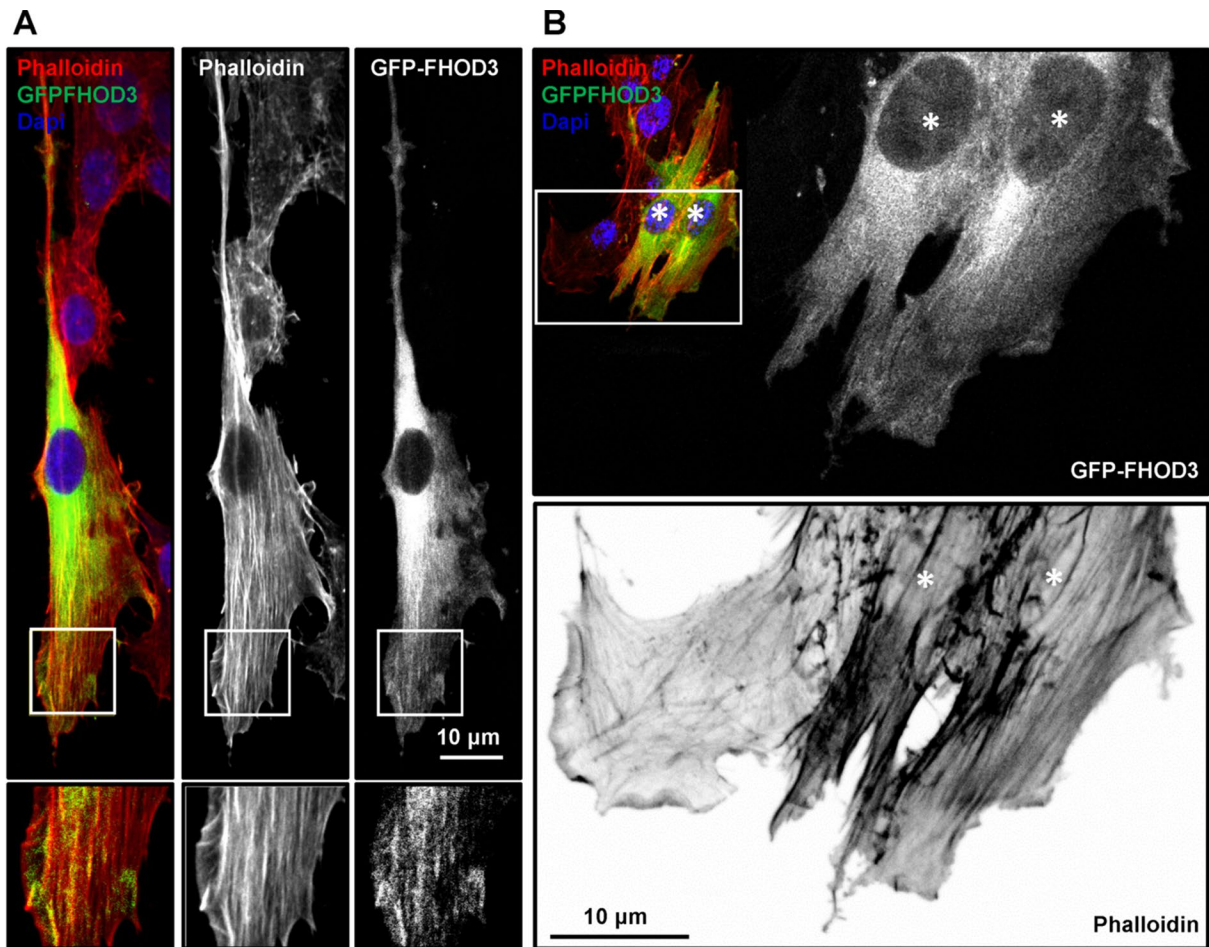


FIGURE 8: GFP-FHOD3 localizes on parallel actin filaments found in leading processes. C6 glioma cells were transfected with GFP-FHOD3 and seeded on 20- μ m laminin micropatterned lines (A) and 2D substrates (B). Cells were fixed and stained with phalloidin and 4',6-diamidino-2-phenylindole and imaged using a confocal microscope. (B) GFP-FHOD3-overexpressing cells (asterisks) among untransfected cells display excessive amounts of longitudinal actin bundles. Scale bars, 10 μ m.

linear migration mode is significantly different from the amoeboid movement of tumor cells or migration of fibroblasts in two dimensions and is more related to *in vivo* neuronal migration (Ayala *et al.*, 2007) or fibroblast migration on fibronectin or gelatin lines (Doyle *et al.*, 2009, 2012; Guo and Wang, 2012; Chang *et al.*, 2013). Most surprising is the finding that inhibition of actin polymerization by the Arp2/3 inhibitor causes an increase in the velocity of migration, whereas the formin inhibitor blocks movement. We tested the involvement of three formins—mDia1, mDia2, and FHOD3—in this process and found that only FHOD3 knockdown led to a consistent inhibition of the linear migration.

Migratory tumor cells often follow preexisting structures and interfaces in tissues. The dimensionality (two dimensions, linear, three dimensions), the surface coating, and the type of adhesions involved will determine the speed and the mode of tumor spreading. These various tracks and interfaces can be mimicked using biophysical tools such as micropatterns, collagen microtracks, electrospun fibers, microchannels, hydrogels, microfluidic devices, tapered microtracks, and so on, and different modes of motility have been described that depend on cell type and environment (Irimia and Toner, 2009; Pathak and Kumar, 2012; Chang *et al.*, 2013; Kraning-Rush *et al.*, 2013; Rape and Kumar, 2014; Vargas *et al.*, 2014; Carey *et al.*, 2015; Liu *et al.*, 2015; Thomas *et al.*, 2015). For example, on collagen

microtracks, metastatic breast cancer cell migration is independent of matrix metalloproteinases and of integrin β 1 but dependent on myosin II, actin, and microtubules (Kraning-Rush *et al.*, 2013; Carey *et al.*, 2015). Microfluidic 3D invasion devices have been used to demonstrate that nonmuscle myosin IIB but not IIA is required for the squeezing of the nuclei of carcinoma cells during 3D migration (Thomas *et al.*, 2015). Using a mix of thin lines connected to rectangles, Chang *et al.* (2013) reported that normal fibroblasts prefer a 2D environment and changed direction when meeting the thin lines, whereas Ras-transformed fibroblasts seemed to not “feel” the topology differences and kept moving persistently from the 2D regions to the lines. Similarly, in our assays, we did not observe any reluctance from the glioma cells to invade the lines from the reservoirs.

Glioma cells use the surface of brain blood vessels to move rapidly throughout the cortex. Brain blood vessels provide a natural linear geometry. Their diameter can vary from 5 to 10 μ m for the small capillaries to several millimeters for the main arteries, presenting hundreds of miles of various linear tracks available for glioma cells to invade. All blood vessels are lined with a basement membrane composed mainly of laminin. Laminin on brain blood vessels is provided by surrounding astrocytes and endothelial cells, but glioma cells also can secrete their own laminin (Cuddapah *et al.*, 2014). Blood vessels can attract glioma by supplying rapid access to

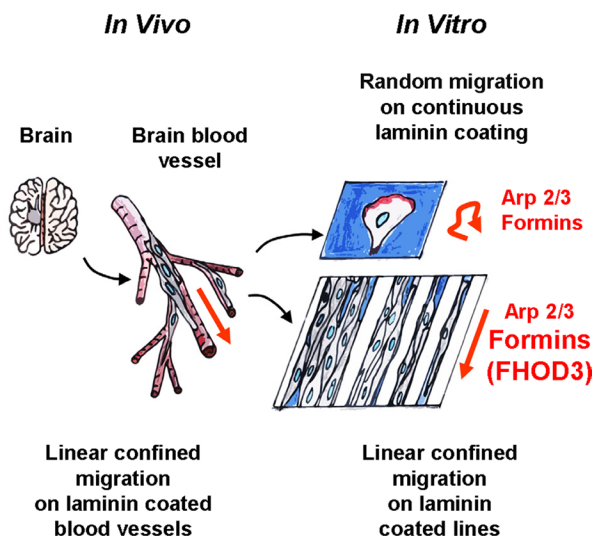


FIGURE 9: Artificial laminin tracks mimic brain blood vessel tracks and allow observations of glioma linear confined migration. Glioma cells follow linear paths coated with laminin, such as the surface of blood vessels, to invade the brain. On these paths, glioma cells use a linear confined saltatory migration. To mimic this type of motility, glioma cells are confined on artificial linear tracks, allowing long-term imaging and high-resolution microscopy. Along these tracks, glioma cells switch from 2D random motion dependent on Arp2/3 and formins (including mDia1 and FHOD3) to efficient linear migration that depends only on formins, including the formin FHOD3, which generates the actin bundles necessary for this linear motility. During this linear migration, antiparallel streams of cells are observed along the axis of the laminin tracks. Within these streams, each individual cell moves by a two-phase saltatory process similar to in vivo saltatory migration.

diffusible nutrients and oxygen and also by secreting soluble factors such as bradykinin and HIF1 α (Cuddapah *et al.*, 2014). Glioma cells accumulate around blood vessels, lift off the astrocytic feet, and proliferate rapidly, leading to a complete encasement of the blood vessels (Nagano *et al.*, 1993; Zagzag *et al.*, 2000; Lugassy *et al.*, 2002; Farin *et al.*, 2006; Winkler *et al.*, 2009). In our assays, on micropatterned lines coated with laminin, individual cells move by a two-phase saltatory process that depends on microtubules and contractile actin bundles in a process similar to their in vivo saltatory migration (Farin *et al.*, 2006; Beadle *et al.*, 2008; Ivkovic *et al.*, 2012). The factors that activate the linear migration mode are consistent with the expected environment of the surface of the brain blood vessels: increased cell density, linear geometry, and laminin. Similar to their behavior on our micropatterned laminin tracks, C6 glioma cells adopt a linear migration mode on brain blood vessels (Hirata *et al.*, 2012). They display a similar spindle shape and migrate more efficiently than isolated cells migrating in the parenchyma, which display multiple motility processes. In the linear migration mode, C6 cells align parallel to each other along the axis of the blood vessels (Hirata *et al.*, 2012) and display the same saltatory motion dependent on myosin 2 activity (Gillespie *et al.*, 1999; Farin *et al.*, 2006; Beadle *et al.*, 2008; Ivkovic *et al.*, 2012). Thus analysis of the linear migration mode in vitro with linear laminin matrices can aid in understanding the in vivo motility on blood vessels.

Other groups have used different tools to mimic the brain environment of glioma cells (Rape *et al.*, 2014). Electrospun nanofibers coated with collagen, hyaluronic acid, fibronectin, or Matrigel have been used to mimic white matter tracks. On these fibers, glioma cells adopt a spindle-shaped, elongated morphology similar to the

in vivo situation and to their morphology on laminin-coated lines. Their migration is extremely slow, however, unlike on the laminin lines (Johnson *et al.*, 2009; Agudelo-Garcia *et al.*, 2011; Rao *et al.*, 2013). Using polyacrylamide microchannels that allow the tuning of their stiffness and size, Pathak and Kumar (2012) found that U373 glioma cells migrate better in stiff, narrow channels coated with fibronectin than in larger channels. In these channels, cells develop longitudinal actin bundles parallel to the axis of the channel, similar to the bundles we observe in C6 glioma migrating on laminin-coated lines. Composite hydrogels made of fibronectin and hyaluronic acid mimic the interface of blood vessel–parenchyma in a 2D configuration. In that configuration, hyaluronic acid inhibits glioma motility (Rape and Kumar, 2014). Cha *et al.* (2014) found that thin, tapered microtracks coated with laminin allow glioma cells to move in a saltatory motion, similar to our observations. In all of these systems, single, isolated glioma cells adopt a spindle shape (Johnson *et al.*, 2009; Agudelo-Garcia *et al.*, 2011; Rao *et al.*, 2013) and a saltatory mode of motility (Cha *et al.*, 2014), with actin bundles parallel to the axis of the lines (Pathak and Kumar, 2012). Thus the cell shape we observe in both linear and crowded environments is similar to previous results on linear substrates, but rates of movement are faster with laminin or very high confinement (Pathak and Kumar, 2012).

In linear migration, there is a loss of polarity in the absence of microtubules, which indicates that microtubule transport of components is necessary for one end of the cell to establish polarity. Microtubules could also participate directly in the extension of the leading process by continuously affecting the leading edge, as shown in carcinoma cells moving in collagen-coated microchannels (Balzer *et al.*, 2012). Doyle *et al.* (2009) also reported that microtubules were required and found a large quantity of stabilized microtubules in the elongated fibroblasts migrating on thin lines, similar to stabilized microtubules of neurons required for axon maintenance (Shea, 1999). Thus the role of microtubules in polarization is not well understood but appears fundamental to linear migration.

Linear migration on laminin depends greatly on actin dynamics, as shown by the results with latrunculin A. Because Arp2/3 is one of the most important players in actin polymerization, it is important to show its role in this motility. Although Arp2/3 activity is present in the linear migration mode, inhibition of Arp2/3 increases cell velocity, indicating that Arp2/3-dependent extensions detract from directed migration and could be involved in sensing the environment. Consistent with that hypothesis, inhibition of Arp2/3 activity causes better alignment of the glioma cells along the lines and parallel to each other. This alignment appears to support the increase in the mean velocity, since cells spend more time moving compared with the control. Similarly, Arp2/3 inhibition accelerates migration of leukocytes in confined conditions, and hence the Arp2/3 lamellipodial protrusions are not required for this other type of confined migration. However, upon Arp2/3 inhibition, instead of forming sharp spindles, leukocytes switch to a blebbing motility (Wilson *et al.*, 2013). In glioma cells, at the subcellular level, the inhibition of Arp2/3 increases the formation of parallel actin cables, reinforcing the sharp, spindle shape of the cells. These cables probably originate from formin activity, since the formin inhibitor SMIFH2 causes loss of the spindle shape. Formin-family proteins regulate cytoskeletal organization both directly via actin interactions and indirectly via regulatory proteins. They can nucleate, polymerize, and (in some cases) bundle actin filaments (Higgs, 2005; Kovar, 2006; Pollard, 2007; Paul and Pollard, 2008; Campellone and Welch, 2010). Activation of the formins in the gliomas is not well understood. We found that FHOD3 is involved in linear migration, but additional formins might be involved as well. The localization of FHOD3 suggests that

it could participate in the extensive bundling of actin filaments along the leading process similar to its function in muscle cells (Iskratsch *et al.*, 2010; Kan-o *et al.*, 2012; Iskratsch *et al.*, 2013). Along with FHOD3, actin bundling proteins such as fascin, which also organize actin filaments in parallel bundles, can promote glioma migration *in vitro* and *in vivo* (Hwang *et al.*, 2008). During the course of our study, Paul *et al.* (2015) published results on the importance of FHOD3 in promoting Arp2/3-independent carcinoma cell invasion into fibronectin-rich 3D ECM. In that case, cells form dynamic actin spikes that could be generated by the same machinery as the leading processes formed by glioma cells on laminin tracks. Other formins could be also involved in glioma linear migration, including mDia1 and mDia2, which could actually compensate for each other, as suggested in other processes (Tominaga *et al.*, 2000; Kato *et al.*, 2001; Riveline *et al.*, 2001; Peng *et al.*, 2003; Faix and Grosse, 2006; Hotulainen and Lappalainen, 2006; Gupton *et al.*, 2007). The localization of mDia2 at the tip of the leading process and the advancing ends of actin cables indicates that mDia2 could nucleate new filaments from the edge of the leading process in a similar manner to filopodia extension (Yang *et al.*, 2007; Supplemental Figure S6C). Formin can be activated via several pathways, including the activation of Rho GTPases (Chesarone *et al.*, 2010; Schonichen and Geyer, 2010; Young and Copeland, 2010; Bogdan *et al.*, 2013). During linear migration, topology- and density-sensing receptors must activate formin pathways of motility and inhibit some Arp2/3-dependent pathways, allowing cells to adopt a spindle shape by organizing actin filaments in parallel arrays.

Several lines of evidence indicate that N-cadherin plays a role as a density sensor and triggers Arp2/3 inhibition. Supporting this hypothesis, N-cadherin activity leads to the inhibition of Rac1 (Theveneau *et al.*, 2010). Rac1 GTPase activity is low in glioma cells migrating rapidly on blood vessels compared with glioma cells migrating slowly in the parenchyma (Hirata *et al.*, 2012), and Hung *et al.* (2013) found that Rac1 inhibition favors cell migration in confined spaces. Similarly, Doyle *et al.* (2009) found that fibroblast migration on thin lines is unaffected or potentiated by Rac knockdown. Low Rac1 GTPase activity could cause partial inhibition of the Arp2/3 complex, which would increase the velocity of linear migration. Hepatocyte growth factor-treated Madin–Darby canine kidney cells express N-cadherin instead of E-cadherin, lowering their cell-to-cell adhesion, and as a consequence, cells migrate in parallel arrays in three dimensions, displaying sharp, spindle shapes and contain parallel actin cables similar to glioma cells during linear migration in our experiments (Shih and Yamada, 2012a,b). Moreover, wound-healing experiments indicate that N-cadherin plays a role in glioma migration (Camand *et al.*, 2012). This implies that N-cadherin could be involved as a density sensor and activate the linear migration by inhibiting Rac and Arp2/3 activity.

Another aspect of linear migration is that low cell–cell adhesion allows the cells to move efficiently in a crowded environment. Unlike E-cadherin-expressing epithelial cells, which, on similar micropatterns, migrate in the same direction (Worley *et al.*, 2015), glioma cells move as single, isolated cells in opposite directions on both sides of the lines and keep passing each other. This observation is extremely relevant to the glioma situation, since glioma cells proliferate along blood vessels, creating an extremely dense environment. Using micropatterns, Leong *et al.* (2013) found that fibroblasts migrating on the sides of large lines adopt a spindle shape and migrate in a similar manner as on thin lines and suggested that an increase in cell density promotes cell migration. Further, using hybrid patterns of grooves and flat surfaces, Londono *et al.* (2014) found that steric mechanical interactions due to high cell density were

sufficient to propagate guidance signals. Similar parallel organization has been described for glioma cells *in vitro* and other cancer cells in 3D matrices (Deisboeck and Couzin, 2009; Shih and Yamada, 2012a,b). At high density, glioma cells can organize in parallel arrays spontaneously in tissue culture dishes (Benda *et al.*, 1968; Deisboeck and Couzin, 2009). However, the presence of linear geometric cues, such as laminin-coated lines (or blood vessel tracks), greatly promoted the organization of parallel arrays. Unlike the nontransformed cells, gliomas do not stop moving in confluent cultures but instead cooperate by aligning and adopting the linear migration. This means that they influence each other through cell–cell contacts but do not bind strongly, so that cells can still detach easily from each other.

In terms of understanding and possibly inhibiting the dissemination of glioma cells, the distinct nature of the linear migration mode opens the possibility of selectively inhibiting that process. There are several possible approaches, ranging from physical to targeted chemical approaches. For example, Jain *et al.* (2014) used the linear migration properties of glioma cells to trap them into an extracortical cytotoxic hydrogel using linear conduits coated with laminin. However, this approach would not prevent motile cells from invading other parts of the brain. If a distinct molecular pathway in linear migration could be identified, then that pathway could potentially be targeted by a specific inhibitor, since normal adult cell activities are likely to be unaffected by inhibiting this specific type of motility. A better understanding of the linear migration mode will make it easier to design treatments in the future.

In conclusion, we believe that the linear migration mode is a distinct type of motility that can be activated in a number of different cell types, such as fibroblasts and transformed epithelial cells, but is particularly damaging in glioblastoma cells because it causes rapid dissemination of glioma throughout the brain. The linear migration mode is characterized by a two-phase motile process that is activated by a laminin matrix in either a linear topology or a crowded cell environment in which cell–cell adhesion is weak. It requires an unusual balance of actin polymerization systems that emphasizes formins and not Arp2/3. Thus it is potentially a powerful tool for identifying new targets such as FHOD3.

MATERIALS AND METHODS

Cell culture and transfections

C6 rat glioma cells were obtained from the American Type Culture Collection (Manassas, VA) and grown in high-glucose DMEM supplemented with 10% heat-inactivated fetal bovine serum and glutamine (Invitrogen, Carlsbad, CA). Graded brain tumor specimens were obtained with informed consent as part of a study protocol approved by the SingHealth Centralised Institutional Review Board. hGPCs were isolated and cultured as described previously (Chong *et al.*, 2009) as tumor spheres in high-glucose DMEM/F-12 (3:1) supplemented with sodium pyruvate, nonessential amino acids, penicillin/streptomycin, B27 supplement (Invitrogen), basic fibroblast growth factor (bFGF; 20 ng/ml), epidermal growth factor (EGF; 20 ng/ml; Gene-Ethics (Asia), Singapore), and heparin (5 µg/ml; Sigma-Aldrich, St. Louis, MO). For transfection and migration assays, hGPCs were cultured as monolayers on laminin (10 µg/ml)-coated Petri dishes for several days before transfection. HGPCs and C6 transfections were performed with a Neon electroporator (Invitrogen) as per manufacturer's recommendations.

Reagents

mCherry paxillin cDNA was from Clare Waterman (National Heart, Lung, and Blood Institute, Bethesda, MD), PM-GFP (plasma

membrane marker) cDNA was from Sergio Grinstein (University of Toronto, Toronto, Canada), Arp3-pmCherryC1 was a gift from Christian Merrifield (Medical Research Council Laboratory of Molecular Biology, Cambridge, United Kingdom; Addgene plasmid #27682; Addgene; Taylor *et al.*, 2011), and GFP-mDia2 cDNA was from Alexander Bershadsky (MBI, Singapore). GFP-FHOD3 cDNA was from Elisabeth Ehler (King's College London, United Kingdom). Laminin, collagen, and fibronectin were from Roche Applied Science (Penzberg, Germany). Poly-L-lysine (0.01% solution), (-)-blebbistatin, latrunculin A, nocodazole, and CK666 were from Sigma-Aldrich. Formin inhibitor SMIFH2 was obtained from Hit2Lead.com (San Diego, CA). Alexa Fluor 568-phalloidin was obtained from Invitrogen. Far Red-conjugated phalloidin was from Biotium (Hayward, CA). Rabbit anti-mDia2 antibody (DP3491) was from ECM Biosciences (Versailles, KY), monoclonal anti-mDia1 antibody (610848) was from BD biosciences (Franklin Lakes, NJ), rabbit anti-FMNL1 (ab97456) and anti-FMNL2 antibodies (ab72105) were from Abcam (Cambridge, England); rabbit anti-FHOD1 (SAB4200147), rabbit anti-FHOD3 (AV463242), and mouse anti-tubulin (T9026) antibodies were from Sigma-Aldrich, and phospho-myosin light chain 2 (Ser-19) antibody (#3671) was from Cell Signaling (Danvers, MA).

Immunofluorescence

For analysis of endogenous FHOD3 and phospho-myosin light chain 2, C6 cells grown on laminin patterns were fixed and stained as previously described (Beadle *et al.*, 2008).

Groove microfabrication and micropatterning

Lines of 3–400 μm were printed on non-culture-treated Petri dishes using microcontact printing as previously described (Fink *et al.*, 2007; Vedula *et al.*, 2012). To follow GFP-PM-transfected cells and label F-actin and formins, stamps were performed on hydrophobic, uncoated Ibidi dishes (Ibidi, Munich, Germany) instead of Petri dishes. To follow isolated cells with TIRF imaging, 2- to 5- μm lines were printed on glass coverslips using a deep ultraviolet photopatterning technique as in Azioune *et al.* (2010). Cells were incubated for 5 min with Hoechst 33342 (Sigma-Aldrich) to label the nuclei, seeded on the patterns, and incubated at 37°C. At 30–60 min later, the Petri dish was rinsed with culture medium to remove floating cells. Cell imaging typically started within the next hour. Silicon molds for the 2 μm \times 2 μm \times 2 μm linear grooves were prepared using standard lithography techniques. The linear grooves were transferred to polystyrene by nanoimprinting. Soft lithography was done using the Sylgard 184 Silicone Elastomer kit (1:10 ratio; Dow Corning, Auburn, MI) on the polystyrene hard mold. After demolding, the samples were plasma cleaned and prepared as previously described (Tan *et al.*, 2015). Scanning electron microscopy (SEM) and cross-sectional SEM of the polydimethylsiloxane (PDMS) samples were done by sputter coating the samples at 30 mA for 30 s and imaging them at high vacuum using a JSM-6010LV-JEOL microscope (JEOL USA, Huntington Beach, CA).

Microscopy

Long-term imaging was done using an Olympus IX81 microscope equipped with temperature, humidity, and CO₂ control (Olympus, Tokyo, Japan) or a biostation (Nikon, Melville, NY). Acquisitions were typically obtained over a period from 12 to 24 h using 10 \times or 20 \times objectives. TIRF images were obtained through a 60 \times oil immersion objective with an iLas2 TIRF system connected to an Olympus IX81 microscope equipped with temperature, humidity, and CO₂ control. Confocal images of phalloidin, phospho-myosin, GFP-mDia2, and FHOD3 were obtained using an LSM710

confocal microscope (Zeiss, Jena, Germany) with a 63 \times water objective.

shRNA design and cloning

shRNAs against rat and human mDia1 and rat mDia2 were designed to target 19 nucleotide sequences and cloned into the *Bam*H1 and *Hind*III cloning site of pRNAT-U6/Neo vector (GenScript, Piscataway, NJ), which also contains a GFP marker under a cytomegalovirus promoter control. PAGE-purified oligos (mDia1-human shRNA forward, 5'-GAT CCC GCA GAA GCT TCA AGA TCT TTT CAA GAG AAA GAT CTT GAA GCT TCT GCT TTT TTC CAA A-3', and reverse, 5'-AGC TTT TGG AAA AAA GCA GAA GCT TCA AGA TCT TTC TCT TGA AAA GAT CTT GAA GCT TCT GCG G-3'; mDia1-rat shRNA forward, 5'-GAT CCC GCC AGA GGA CAT GAA TGA ATT CAA GAG ATT CAT TCA TGT CCT CTG GCT TTT TTC CAA A-3', and reverse, 5'-AGC TTT TGG AAA AAA GCC AGA GGA CAT GAA TGA ATC TCT TGA ATT CAT TCA TGT CCT CTG GCG G-3'; mDia2-rat-shRNA forward, 5'-GAT CCC GAT CGG ACC AAA TGA AAT GTT CAA GAG ACA TTT CAT TTG GTC CGA TCT TTT TTC CAA A-3', and reverse 5'-AGC TTT TGG AAA AAA GAT CGG ACC AAA TGA AAT GTC TCT TGA ACA TTT CAT TTG GTC CGA TCG G-3') were obtained from Integrated DNA Technologies (Coralville, IA). Forward and reverse oligonucleotides, 0.5 nmol, were diluted to 20 μl in water, incubated for 4 min at 94°C, and slowly cooled to 4°C. Annealed oligos were ligated into the *Bam*H1 and *Hind*III restriction sites of pRNAT-U6/Neo vector. Successful cloning was confirmed by sequencing. shRNAs against human mDia2 cloned in pGFP-V-RS plasmids under U6 promoter were obtained from OriGene Technologies (Rockville, MD), and shRNAs against human and rat FHOD3 and control were obtained from Thomas Iskratsch (Columbia University, New York, NY; Iskratsch *et al.*, 2010).

Tracking and statistical analysis

Cells bodies were manually tracked using the manual tracking plug-in of Fiji (ImageJ; National Institutes of Health, Bethesda, MD). Lengths of the tracks were used to calculate the mean speeds (distance/time). Imaris software (Bitplane, Zurich, Switzerland) was used to measure cell density over time. GraphPad Prism (GraphPad Software, La Jolla, CA) was used for statistical analysis. The *p* values were calculated using unpaired *t* tests. **p* < 0.1, ***p* < 0.01, ****p* < 0.001, and *****p* < 0.0001. Error bars are SEM.

ACKNOWLEDGMENTS

We thank Pascal Hersen, Marius Sudol, and Lieu Zi Zhao (Mechanobiology Institute, National University of Singapore, Singapore) and Thomas Iskratsch (Columbia University, New York, NY) for fruitful discussions and technical assistance. This work was supported by the Mechanobiology Institute, National University of Singapore, and the National Institutes of Health through Columbia University.

REFERENCES

- Agudelo-Garcia PA, De Jesus JK, Williams SP, Nowicki MO, Chiocca EA, Liyanarachchi S, Li PK, Lannutti JJ, Johnson JK, Lawler SE, *et al.* (2011). Glioma cell migration on three-dimensional nanofiber scaffolds is regulated by substrate topography and abolished by inhibition of STAT3 signaling. *Neoplasia* 13, 831–840.
- Ayala R, Shu T, Tsai LH (2007). Trekking across the brain: the journey of neuronal migration. *Cell* 128, 29–43.
- Azioune A, Carpi N, Tseng Q, Thery M, Piel M (2010). Protein micropatterns: a direct printing protocol using deep UVs. *Methods Cell Biol* 97, 133–146.

- Balzer EM, Tong Z, Paul CD, Hung WC, Stroka KM, Boggs AE, Martin SS, Konstantopoulos K (2012). Physical confinement alters tumor cell adhesion and migration phenotypes. *FASEB J* 26, 4045–4056.
- Beadle C, Assanah MC, Monzo P, Vallee R, Rosenfeld SS, Canoll P (2008). The role of myosin II in glioma invasion of the brain. *Mol Biol Cell* 19, 3357–3368.
- Beauchesne P (2011). Extra-neural metastases of malignant gliomas: myth or reality? *Cancers* 3, 461–477.
- Bellail AC, Hunter SB, Brat DJ, Tan C, Van Meir EG (2004). Microregional extracellular matrix heterogeneity in brain modulates glioma cell invasion. *Int J Biochem Cell Biol* 36, 1046–1069.
- Bellon G, Caulet T, Cam Y, Pluot M, Poulin G, Pytlinska M, Bernard MH (1985). Immunohistochemical localisation of macromolecules of the basement membrane and extracellular matrix of human gliomas and meningiomas. *Acta Neuropathol* 66, 245–252.
- Belot N, Rorive S, Doyen I, Lefranc F, Bruyneel E, Dedecker R, Micik S, Brotchi J, Decaestecker C, Salmon I, et al. (2001). Molecular characterization of cell substratum attachments in human glial tumors relates to prognostic features. *Glia* 36, 375–390.
- Benda P, Lightbody J, Sato G, Levine L, Sweet W (1968). Differentiated rat glial cell strain in tissue culture. *Science* 161, 370–371.
- Bernstein JJ, Woodard CA (1995). Glioblastoma cells do not intravasate into blood vessels. *Neurosurgery* 36, 124–132, discussion, 132.
- Bogdan S, Schultz J, Grosshans J (2013). Formin' cellular structures: physiological roles of Diaphanous (Dia) in actin dynamics. *Commun Integr Biol* 6, e27634.
- Camand E, Peglion F, Osmani N, Sanson M, Etienne-Manneville S (2012). N-cadherin expression level modulates integrin-mediated polarity and strongly impacts on the speed and directionality of glial cell migration. *J Cell Sci* 125, 844–857.
- Campellone KG, Welch MD (2010). A nucleator arms race: cellular control of actin assembly. *Nat Rev Mol Cell Biol* 11, 237–251.
- Carey SP, Rahman A, Kraning-Rush CM, Romero B, Somasegar S, Torre OM, Williams RM, Reinhart-King CA (2015). Comparative mechanisms of cancer cell migration through 3D matrix and physiological microtracks. *Am J Physiol Cell Physiol* 308, C436–C447.
- Cha J, Koh I, Choi Y, Lee J, Choi C, Kim P (2014). Tapered microtract array platform for antimigratory drug screening of human glioblastoma multiforme. *Adv Healthc Mater* 4, 405–411.
- Chang SS, Guo WH, Kim Y, Wang YL (2013). Guidance of cell migration by substrate dimension. *Biophys J* 104, 313–321.
- Charles NA, Holland EC, Gilbertson R, Glass R, Kettenmann H (2012). The brain tumor microenvironment. *Glia* 60, 502–514.
- Chesarone MA, DuPage AG, Goode BL (2010). Unleashing formins to remodel the actin and microtubule cytoskeletons. *Nat Rev Mol Cell Biol* 11, 62–74.
- Chintala SK, Sawaya R, Gokaslan ZL, Fuller G, Rao JS (1996). Immunohistochemical localization of extracellular matrix proteins in human glioma, both in vivo and in vitro. *Cancer Lett* 101, 107–114.
- Chong YK, Sandanaraj E, Koh LW, Thangaveloo M, Tan MS, Koh GR, Toh TB, Lim GG, Holbrook JD, Kon OL, et al. (2015). ST3GAL1-associated transcriptomic program in glioblastoma tumor growth, invasion, and prognosis. *J Natl Cancer Inst* 108, djv326.
- Chong YK, Toh TB, Zaiden N, Poonepalli A, Leong SH, Ong CE, Yu Y, Tan PB, See SJ, Ng WH, et al. (2009). Cryopreservation of neurospheres derived from human glioblastoma multiforme. *Stem Cells* 27, 29–39.
- Clark P, Connolly P, Curtis AS, Dow JA, Wilkinson CD (1990). Topographical control of cell behaviour: II. Multiple grooved substrata. *Development* 108, 635–644.
- Cloughesy TF, Cavenee WK, Mischel PS (2014). Glioblastoma: from molecular pathology to targeted treatment. *Annu Rev Pathol* 9, 1–25.
- Cuddapah VA, Robel S, Watkins S, Sontheimer H (2014). A neurocentric perspective on glioma invasion. *Nat Rev Neurosci* 15, 455–465.
- Curtis A, Wilkinson C (1997). Topographical control of cells. *Biomaterials* 18, 1573–1583.
- Dalton BA, Walboomers XF, Dziegielewski M, Evans MD, Taylor S, Jansen JA, Steele JG (2001). Modulation of epithelial tissue and cell migration by microgrooves. *J Biomed Mater Res* 56, 195–207.
- Deisboeck TS, Couzin ID (2009). Collective behavior in cancer cell populations. *Bioessays* 31, 190–197.
- Delamarre E, Taboubi S, Mathieu S, Berenguer C, Rigot V, Lissitzky JC, Figarella-Branger D, Ouafik L, Luis J (2009). Expression of integrin alpha6beta1 enhances tumorigenesis in glioma cells. *Am J Pathol* 175, 844–855.
- Doyle AD, Kutys ML, Conti MA, Matsumoto K, Adelstein RS, Yamada KM (2012). Micro-environmental control of cell migration—myosin IIA is required for efficient migration in fibrillar environments through control of cell adhesion dynamics. *J Cell Sci* 125, 2244–2256.
- Doyle AD, Wang FW, Matsumoto K, Yamada KM (2009). One-dimensional topography underlies three-dimensional fibrillar cell migration. *J Cell Biol* 184, 481–490.
- Faix J, Grosse R (2006). Staying in shape with formins. *Dev Cell* 10, 693–706.
- Farin A, Suzuki SO, Weiker M, Goldman JE, Bruce JN, Canoll P (2006). Transplanted glioma cells migrate and proliferate on host brain vasculature: a dynamic analysis. *Glia* 53, 799–808.
- Fink J, Thery M, Azioune A, Dupont R, Chatelain F, Bornens M, Piel M (2007). Comparative study and improvement of current cell micro-patterning techniques. *Lab Chip* 7, 672–680.
- Friedl P, Alexander S (2011). Cancer invasion and the microenvironment: plasticity and reciprocity. *Cell* 147, 992–1009.
- Giese A, Bjerkvig R, Berens ME, Westphal M (2003). Cost of migration: invasion of malignant gliomas and implications for treatment. *J Clin Oncol* 21, 1624–1636.
- Gillespie GY, Soroceanu L, Manning TJ Jr, Gladson CL, Rosenfeld SS (1999). Glioma migration can be blocked by nontoxic inhibitors of myosin II. *Cancer Res* 59, 2076–2082.
- Gingras MC, Roussel E, Bruner JM, Branch CD, Moser RP (1995). Comparison of cell adhesion molecule expression between glioblastoma multiforme and autologous normal brain tissue. *J Neuroimmunol* 57, 143–153.
- Gladson CL (1999). The extracellular matrix of gliomas: modulation of cell function. *J Neuropathol Exp Neurol* 58, 1029–1040.
- Goldbrunner RH, Bernstein JJ, Tonn JC (1999). Cell-extracellular matrix interaction in glioma invasion. *Acta Neurochir (Wien)* 141, 295–305; discussion, 304–295.
- Grau SJ, Trillsch F, Tonn JC, Goldbrunner RH, Noessner E, Nelson PJ, von Luettichau I (2015). Podoplanin increases migration and angiogenesis in malignant glioma. *Int J Clin Exp Pathol* 8, 8663–8670.
- Grobben B, De Deyn PP, Slegers H (2002). Rat C6 glioma as experimental model system for the study of glioblastoma growth and invasion. *Cell Tissue Res* 310, 257–270.
- Guo WH, Wang YL (2012). A three-component mechanism for fibroblast migration with a contractile cell body that couples a myosin II-independent propulsive anterior to a myosin II-dependent resistive tail. *Mol Biol Cell* 23, 1657–1663.
- Gupton SL, Eisenmann K, Alberts AS, Waterman-Storer CM (2007). mDia2 regulates actin and focal adhesion dynamics and organization in the lamella for efficient epithelial cell migration. *J Cell Sci* 120, 3475–3487.
- Hamilton DW, Oates CJ, Hasanzadeh A, Mittler S (2010). Migration of periodontal ligament fibroblasts on nanometric topographical patterns: influence of filopodia and focal adhesions on contact guidance. *PLoS One* 5, e15129.
- Hamilton JD, Rapp M, Marcel Schneiderhan T, Sabel M, Hayman A, Scherer A, Kröppel P, Budach W, Kretschmar U, Arne Gerber P, et al. (2014). Glioblastoma multiforme metastasis outside the CNS: three case reports and possible mechanisms of escape. *J Clin Oncol* 32, e80–e84.
- Haugland HK, Tysnes BB, Tysnes OB (1997). Adhesion and migration of human glioma cells are differently dependent on extracellular matrix molecules. *Anticancer Res* 17, 1035–1042.
- Higgs HN (2005). Formin proteins: a domain-based approach. *Trends Biochem Sci* 30, 342–353.
- Hirata E, Yukinaga H, Kamioka Y, Arakawa Y, Miyamoto S, Okada T, Sahai E, Matsuda M (2012). In vivo fluorescence resonance energy transfer imaging reveals differential activation of Rho-family GTPases in glioblastoma cell invasion. *J Cell Sci* 125, 858–868.
- Holash J, Maisonpierre PC, Compton D, Boland P, Alexander CR, Zagzag D, Yancopoulos GD, Wiegand SJ (1999). Vessel cooption, regression, and growth in tumors mediated by angiopoietins and VEGF. *Science* 284, 1994–1998.
- Hotulainen P, Lappalainen P (2006). Stress fibers are generated by two distinct actin assembly mechanisms in motile cells. *J Cell Biol* 173, 383–394.
- Hung W-C, Chen S-H, Paul CD, Stroka KM, Lo Y-C, Yang JT, Konstantopoulos K (2013). Distinct signaling mechanisms regulate migration in unconfined versus confined spaces. *J Cell Biol* 202, 807–824.
- Hwang JH, Smith CA, Salhia B, Rutka JT (2008). The role of fascin in the migration and invasiveness of malignant glioma cells. *Neoplasia* 10, 149–159.
- Irimia D, Toner M (2009). Spontaneous migration of cancer cells under conditions of mechanical confinement. *Integr Biol (Camb)* 1, 506–512.

- Iskratsch T, Lange S, Dwyer J, Kho AL, dos Remedios C, Ehler E (2010). Formin follows function: a muscle-specific isoform of FHOD3 is regulated by CK2 phosphorylation and promotes myofibril maintenance. *J Cell Biol* 191, 1159–1172.
- Iskratsch T, Reijntjes S, Dwyer J, Toselli P, Degano IR, Dominguez I, Ehler E (2013). Two distinct phosphorylation events govern the function of muscle FHOD3. *Cell Mol Life Sci* 70, 893–908.
- Ivkovic S, Beadle C, Noticewala S, Massey SC, Swanson KR, Toro LN, Bresnick AR, Canoll P, Rosenfeld SS (2012). Direct inhibition of myosin II effectively blocks glioma invasion in the presence of multiple motogens. *Mol Biol Cell* 23, 533–542.
- Jain A, Betancur M, Patel GD, Valmikinathan CM, Mukhatyar VJ, Vakharia A, Pai SB, Brahma B, Macdonald TJ, Bellamkonda RV (2014). Guiding intracortical brain tumour cells to an extracellular cytotoxic hydrogel using aligned polymeric nanofibres. *Nat Mater* 13, 308–316.
- Johnson J, Nowicki MO, Lee CH, Chiocca EA, Viapiano MS, Lawler SE, Lannutti JJ (2009). Quantitative analysis of complex glioma cell migration on electrospun polycaprolactone using time-lapse microscopy. *Tissue Eng Part C Methods* 15, 531–540.
- Jones TR, Ruoslahti E, Schold SC, Bigner DD (1982). Fibronectin and glial fibrillary acidic protein expression in normal human brain and anaplastic human gliomas. *Cancer Res* 42, 168–177.
- Kan-o M, Takeya R, Taniguchi K, Tanoue Y, Tominaga R, Sumimoto H (2012). Expression and subcellular localization of mammalian formin Fhod3 in the embryonic and adult heart. *PLoS One* 7, e34765.
- Kato T, Watanabe N, Morishima Y, Fujita A, Ishizaki T, Narumiya S (2001). Localization of a mammalian homolog of diaphanous, mDia1, to the mitotic spindle in HeLa cells. *J Cell Sci* 114, 775–784.
- Keil R, Kießling C, Hatzfeld M (2009). Targeting of p0071 to the midbody depends on KIF3. *J Cell Sci* 122, 1174–1183.
- Knott JC, Mahesparan R, Garcia-Cabrera I, Bolge Tysnes B, Edvardsen K, Ness GO, Mork S, Lund-Johansen M, Bjerkvig R (1998). Stimulation of extracellular matrix components in the normal brain by invading glioma cells. *Int J Cancer* 75, 864–872.
- Kovar DR (2006). Molecular details of formin-mediated actin assembly. *Curr Opin Cell Biol* 18, 11–17.
- Kraning-Rush CM, Carey SP, Lampi MC, Reinhart-King CA (2013). Microfabricated collagen tracks facilitate single cell metastatic invasion in 3D. *Integr Biol (Camb)* 5, 606–616.
- Lathia JD, Gallagher J, Heddleston JM, Wang J, Elyer CE, Macswords J, Wu Q, Vasanji A, McLendon RE, Hjelmeland AB, et al. (2010). Integrin alpha 6 regulates glioblastoma stem cells. *Cell Stem Cell* 6, 421–432.
- Leong MC, Vedula SR, Lim CT, Ladoux B (2013). Geometrical constraints and physical crowding direct collective migration of fibroblasts. *Commun Integr Biol* 6, e23197.
- Liu YJ, Le Berre M, Lautenschlaeger F, Maiuri P, Callan-Jones A, Heuze M, Takaki T, Voituriez R, Piel M (2015). Confinement and low adhesion induce fast amoeboid migration of slow mesenchymal cells. *Cell* 160, 659–672.
- Londono C, Loureiro MJ, Slater B, Lucker PB, Soleas J, Sathananthan S, Aitchison JS, Kabla AJ, McGuigan AP (2014). Nonautonomous contact guidance signaling during collective cell migration. *Proc Natl Acad Sci USA* 111, 1807–1812.
- Lugassy C, Haroun RI, Brem H, Tyler BM, Jones RV, Fernandez PM, Patierno SR, Kleinman HK, Barnhill RL (2002). Pericytic-like angiotropism of glioma and melanoma cells. *Am J Dermatopathol* 24, 473–478.
- McComb RD, Bigner DD (1985). Immunolocalization of laminin in neoplasms of the central and peripheral nervous systems. *J Neuropathol Exp Neurol* 44, 242–253.
- Nagano N, Sasaki H, Aoyagi M, Hirakawa K (1993). Invasion of experimental rat brain tumor: early morphological changes following microinjection of C6 glioma cells. *Acta Neuropathol* 86, 117–125.
- Ng FS, Toh TB, Ting EH, Koh GR, Sandanaraj E, Phong M, Wong SS, Leong SH, Kon OL, Tucker-Kellogg G, et al. (2012). Progenitor-like traits contribute to patient survival and prognosis in oligodendroglial tumors. *Clin Cancer Res* 18, 4122–4135.
- Panopoulos A, Howell M, Fotedar R, Margolis RL (2011). Glioblastoma motility occurs in the absence of actin polymer. *Mol Biol Cell* 22, 2212–2220.
- Pathak A, Kumar S (2012). Independent regulation of tumor cell migration by matrix stiffness and confinement. *Proc Natl Acad Sci USA* 109, 10334–10339.
- Paul AS, Pollard TD (2008). The role of the FH1 domain and profilin in formin-mediated actin-filament elongation and nucleation. *Curr Biol* 18, 9–19.
- Paul NR, Allen JL, Chapman A, Morlan-Mairal M, Zindy E, Jacquemet G, Fernandez Del Ama L, Ferizovic N, Green DM, Howe JD, et al. (2015). alpha5beta1 integrin recycling promotes Arp2/3-independent cancer cell invasion via the formin FHOD3. *J Cell Biol* 210, 1013–1031.
- Paulus W, Baur I, Schuppan D, Roggendorf W (1993). Characterization of integrin receptors in normal and neoplastic human brain. *Am J Pathol* 143, 154–163.
- Peng J, Wallar BJ, Flanders A, Swiatek PJ, Alberts AS (2003). Disruption of the Diaphanous-related formin Drf1 gene encoding mDia1 reveals a role for Drf3 as an effector for Cdc42. *Curr Biol* 13, 534–545.
- Pollard TD (2007). Regulation of actin filament assembly by Arp2/3 complex and formins. *Annu Rev Biophys Biomol Struct* 36, 451–477.
- Previtali S, Quattrini A, Nemni R, Truci G, Ducati A, Wrabetz L, Canal N (1996). Alpha6 beta4 and alpha6 beta1 integrins in astrocytomas and other CNS tumors. *J Neuropathol Exp Neurol* 55, 456–465.
- Rao SS, Nelson MT, Xue R, DeJesus JK, Viapiano MS, Lannutti JJ, Sarkar A, Winter JO (2013). Mimicking white matter tract topography using core-shell electrospun nanofibers to examine migration of malignant brain tumors. *Biomaterials* 34, 5181–5190.
- Rape A, Ananthanarayanan B, Kumar S (2014). Engineering strategies to mimic the glioblastoma microenvironment. *Adv Drug Deliv Rev* 79–80, 172–183.
- Rape AD, Kumar S (2014). A composite hydrogel platform for the dissection of tumor cell migration at tissue interfaces. *Biomaterials* 35, 8846–8853.
- Rape AD, Zibinsky M, Murthy N, Kumar S (2015). A synthetic hydrogel for the high-throughput study of cell-ECM interactions. *Nat Commun* 6, 8129.
- Riveline D, Zamir E, Balaban NQ, Schwarz US, Ishizaki T, Narumiya S, Kam Z, Geiger B, Bershadsky AD (2001). Focal contacts as mechanosensors: externally applied local mechanical force induces growth of focal contacts by an mDia1-dependent and rock-independent mechanism. *J Cell Biol* 153, 1175–1186.
- Rizvi SA, Neidt EM, Cui J, Feiger Z, Skau CT, Gardel ML, Kozmin SA, Kovar DR (2009). Identification and characterization of a small molecule inhibitor of formin-mediated actin assembly. *Chem Biol* 16, 1158–1168.
- Schonichen A, Geyer M (2010). Fifteen formins for an actin filament: a molecular view on the regulation of human formins. *Biochim Biophys Acta* 1803, 152–163.
- Shea TB (1999). Selective stabilization of microtubules within the proximal region of developing axonal neurites. *Brain Res Bull* 48, 255–261.
- Shih W, Yamada S (2012a). N-cadherin-mediated cell-cell adhesion promotes cell migration in a three-dimensional matrix. *J Cell Sci* 125, 3661–3670.
- Shih W, Yamada S (2012b). N-cadherin as a key regulator of collective cell migration in a 3D environment. *Cell Adh Migr* 6, 513–517.
- Tan KK, Tann JY, Sathe SR, Goh SH, Ma D, Goh EL, Yim EK (2015). Enhanced differentiation of neural progenitor cells into neurons of the mesencephalic dopaminergic subtype on topographical patterns. *Biomaterials* 43, 32–43.
- Taylor MJ, Perrais D, Merrifield CJ (2011). A high precision survey of the molecular dynamics of mammalian clathrin-mediated endocytosis. *PLoS Biol* 9, e1000604.
- Teixeira AI, Abrams GA, Bertics PJ, Murphy CJ, Nealey PF (2003). Epithelial contact guidance on well-defined micro- and nanostructured substrates. *J Cell Sci* 116, 1881–1892.
- Theveneau E, Marchant L, Kuriyama S, Gull M, Moepps B, Parsons M, Mayor R (2010). Collective chemotaxis requires contact-dependent cell polarity. *Dev Cell* 19, 39–53.
- Thomas DG, Yenepalli A, Denais CM, Rape A, Beach JR, Wang YL, Schiemann WP, Baskaran H, Lammerding J, Egelhoff TT (2015). Non-muscle myosin IIb is critical for nuclear translocation during 3D invasion. *J Cell Biol* 210, 583–594.
- Tominaga T, Sahai E, Chardin P, McCormick F, Courtneidge SA, Alberts AS (2000). Diaphanous-related formins bridge Rho GTPase and Src tyrosine kinase signaling. *Mol Cell* 5, 13–25.
- Tysnes BB, Larsen LF, Ness GO, Mahesparan R, Edvardsen K, Garcia-Cabrera I, Bjerkvig R (1996). Stimulation of glioma-cell migration by laminin and inhibition by anti-alpha3 and anti-beta1 integrin antibodies. *Int J Cancer* 67, 777–784.
- Uhm JH, Gladson CL, Rao JS (1999). The role of integrins in the malignant phenotype of gliomas. *Front Biosci* 4, D188–D199.
- Vargas P, Terriac E, Lennon-Dumenil AM, Piel M (2014). Study of cell migration in microfabricated channels. *J Vis Exp* 2014, e51099.
- Vedula SR, Hirata H, Nai MH, Bruges A, Toyama Y, Trepap X, Lim CT, Ladoux B (2014). Epithelial bridges maintain tissue integrity during collective cell migration. *Nat Mater* 13, 87–96.

- Vedula SR, Leong MC, Lai TL, Hersen P, Kabla AJ, Lim CT, Ladoux B (2012). Emerging modes of collective cell migration induced by geometrical constraints. *Proc Natl Acad Sci USA* 109, 12974–12979.
- Wilson K, Lewalle A, Fritzsche M, Thorogate R, Duke T, Charras G (2013). Mechanisms of leading edge protrusion in interstitial migration. *Nat Commun* 4, 2896.
- Winkler F, Kienast Y, Fuhrmann M, Von Baumgarten L, Burgold S, Mitteregger G, Kretschmar H, Herms J (2009). Imaging glioma cell invasion in vivo reveals mechanisms of dissemination and peritumoral angiogenesis. *Glia* 57, 1306–1315.
- Wong SY, Ulrich TA, Deleyrolle LP, MacKay JL, Lin JM, Martuscello RT, Jundi MA, Reynolds BA, Kumar S (2015). Constitutive activation of myosin-dependent contractility sensitizes glioma tumor-initiating cells to mechanical inputs and reduces tissue invasion. *Cancer Res* 75, 1113–1122.
- Worley KE, Shieh D, Wan LQ (2015). Inhibition of cell-cell adhesion impairs directional epithelial migration on micropatterned surfaces. *Integr Biol (Camb)* 7, 580–590.
- Xie Q, Mittal S, Berens ME (2014). Targeting adaptive glioblastoma: an overview of proliferation and invasion. *Neuro Oncol* 16, 1575–1584.
- Yamana N, Arakawa Y, Nishino T, Kurokawa K, Tanji M, Itoh RE, Monypenny J, Ishizaki T, Bito H, Nozaki K, et al. (2006). The Rho-mDia1 pathway regulates cell polarity and focal adhesion turnover in migrating cells through mobilizing Apc and c-Src. *Mol Cell Biol* 26, 6844–6858.
- Yang C, Czech L, Gerboth S, Kojima S, Scita G, Svitkina T (2007). Novel roles of formin mDia2 in lamellipodia and filopodia formation in motile cells. *PLoS Biol* 5, e317.
- Young KG, Copeland JW (2010). Formins in cell signaling. *Biochim Biophys Acta* 1803, 183–190.
- Zagzag D, Amirnovin R, Greco MA, Yee H, Holash J, Wiegand SJ, Zabski S, Yancopoulos GD, Grumet M (2000). Vascular apoptosis and involution in gliomas precede neovascularization: a novel concept for glioma growth and angiogenesis. *Lab Invest* 80, 837–849.
- Zlokovic BV (2008). The blood-brain barrier in health and chronic neurodegenerative disorders. *Neuron* 57, 178–201.